J. Fluid Mech. (1982), *vol.* 125, *pp.* 475–503
Printed in Great Britain

Local isotropy and anisotropy in a high-Reynolds-number turbulent boundary layer

By PATRICE MESTAYER

Institut de Mécanique Statistique de la Turbulence, Laboratoire Associé au C.N.R.S. no. 130, 12 Avenue du Général Leclerc, 13003 Marseille, France

(Received 27 July 1981 and in revised form 19 May 1982)

High-frequency fluctuations of temperature and of longitudinal and vertical velocity components have been measured with high-resolution probes in order to test the local-isotropy assumption. The simultaneous measurements of u', w', θ' and the measurements in two space points with various separations in either the longitudinal or transverse directions were made in the large boundary layer ($R_\lambda = 616$) of the I.M.S.T. Air–Sea Interaction Simulation Tunnel. There is consistent evidence that the local-isotropy assumption is satisfied by the velocity field at all scales smaller than twenty times the Kolmogorov microscale ($\eta \approx 0{\cdot}27 \times 10^{-3}$ m), i.e. in the dissipative range of scales but not in the expected inertial subrange. The direct comparisons of the lateral and longitudinal temperature autocorrelation and structure functions show that the temperature field does not verify the isotropy assumption at all scales greater than or equal to 3η and presumably at even smaller scales. This is confirmed by the study of the temperature-increment skewness and flatness factors. The spectral distribution of the non-zero derivative skewness ($S(\theta) = +0{\cdot}9$) shows that it is essentially contributed by those scales for which the dynamic field satisfies isotropy.

1. Introduction

Local isotropy was introduced by Kolmogorov (1941) as homogeneity plus isotropy of the small scales of turbulent motions, and it remained an implicit assumption in his 1962 refinements. It is a cornerstone of the theory of universal self-similarity, closely connected with the assumption of complete independence of the small-scale structure of the turbulent field from its large-scale structure and mean shears, and also with the random character of the energy cascade. Obukhov (1946) and Corrsin (1952) have extended the assumption to the small scales of scalar fields mixed by turbulence, apparently as a consequence of their properties as passive contaminants.

It is a generally received opinion that these hypotheses are true and are verified over a large range of scales in most turbulent flows. There are at least four reasons for this opinion. Firstly, the hypotheses seem necessary for the self-similarity theory to hold – and this theory seem too coherent and efficient to be wrong. Secondly, local isotropy brings such great simplifications in equations, and also in the experimental estimation of some operators like the dissipation rates of kinetic energy and of scalar variances that could perhaps not be estimated otherwise. Thirdly, in numerous fluid-mechanics problems isotropy has been proved to be a very efficient *first approximation*. And, last but not least, there *seems* to be little experimental evidence against the hypotheses.

Indeed, many an experimentalist since Townsend (1948) has verified some of the relations describing some of the consequences of local isotropy. Conversely, if

experimental evidence against local isotropy appears, then the assumption seems so plausible that instrumental errors and/or shortcomings are usually invoked.

It seems that no complete and accurate experiment has yet been devoted exclusively to investigating the limits of the hypotheses for the dynamic field and for scalar fields in a flow where they have a good chance of being verified. The I.M.S.T. large tunnel has already been proved to be well adapted to obtaining new results in that area (Mestayer *et al.* 1976; Coantic *et al.* 1981). An extensive programme of measurements of high-frequency fluctuations of velocity components and temperature has been carried through in recent years, principally to check the validity of these hypotheses.

This paper recalls first the relations deriving from local isotropy that can be experimentally verified. It reviews a large number of experimental results and the conclusions that can be honestly drawn about the velocity field and the scalar fields. Then it presents measurements of high-frequency fluctuations of u', w' and θ', in one space point or in two space points with various separations, obtained with high-resolution hot-wire and cold-wire probes. The methods employed to process the data are presented. A large number of consequences of local isotropy have been tested with the velocity-component spectral functions, structure functions, autocorrelation functions and microscales. For the temperature field we compared the transverse, longitudinal and time-dependent autocorrelation coefficient and structure functions and the corresponding 'Taylor microscales'. We estimated the spectral distribution of the non-zero derivative skewness factor. We also computed the skewness and flatness factors of the temperature increments. Consequences directly related to local isotropy are discussed. Some other consequences have been omitted for lack of space: they will be discussed in another paper.

2. Theoretical relations

Local isotropy implies that the properties of symmetry of the isotropic fields (Taylor 1935) are satisfied by those operators that are only functions of small scales.

The odd moments of all gradients of temperature $\partial\theta/\partial x_i$ and of the transverse gradients of the velocity components $\partial u_i/\partial x_j (i \neq j)$ should be identically zero. Their even moments should obey relations of the form

$$\overline{\left(\frac{\partial u}{\partial x}\right)^2} = \overline{\left(\frac{\partial v}{\partial y}\right)^2} = \overline{\left(\frac{\partial w}{\partial z}\right)^2} = \frac{1}{2}\overline{\left(\frac{\partial u_i}{\partial x_j}\right)^2}, \tag{1}$$

$$\overline{\frac{\partial u_i}{\partial x_i}\frac{\partial u_i}{\partial x_j}} = 0, \tag{2}$$

with $i \neq j$ and no summation on i and j, and

$$\overline{\left(\frac{\partial \theta}{\partial x}\right)^2} = \overline{\left(\frac{\partial \theta}{\partial y}\right)^2} = \overline{\left(\frac{\partial \theta}{\partial z}\right)^2}, \tag{3}$$

where u, v and w are respectively the x, y and z velocity components in the longitudinal and transverse directions (by analogy with geophysical flows, we use in boundary layers the direction z for the ascending vertical); θ is temperature; the bar indicates a time average, assumed in all this work to be equal to an ensemble average.

As a direct consequence, the longitudinal Taylor microscale λ_x and the lateral Taylor microscales λ_y and λ_z, defined by

$$\lambda_\xi^2 = \frac{2\overline{u_1'^2}}{\overline{(\partial u_i/\partial \xi)^2}} \quad (\xi = x, y, z), \tag{4}$$

should satisfy the relations

$$\lambda_x = \sqrt{2}\,\lambda_y = \sqrt{2}\,\lambda_z. \tag{5}$$

Similarly, the temperature longitudinal $\lambda_{\theta x}$ and lateral $\lambda_{\theta y}$, $\lambda_{\theta z}$ 'Taylor microscales'

$$\lambda_{\theta\xi}^2 = \frac{2\overline{\theta'^2}}{(\partial\theta/\partial\xi)^2} \quad (\xi = x, y, z) \tag{6}$$

should satisfy the relations

$$\lambda_{\theta x} = \lambda_{\theta y} = \lambda_{\theta z}. \tag{7}$$

As another direct consequence, the average rate of dissipation of kinetic energy, defined by

$$\bar{\epsilon} = \nu\overline{\frac{\partial u_i}{\partial x_j}\left(\frac{\partial u_i}{\partial x_j}+\frac{\partial u_j}{\partial x_i}\right)}, \tag{8}$$

where ν is the kinematic viscosity and with summations on i and j, and the average rate of destruction of the temperature variance $\overline{\theta'^2}$, defined by

$$\overline{\chi_\theta} = 2\mathscr{D}_\theta\overline{\frac{\partial\theta}{\partial x_j}\frac{\partial\theta}{\partial x_j}}, \tag{9}$$

where $\mathscr{D}_\theta$ is the molecular diffusivity of temperature, can be estimated from the value of one of the gradients:

$$\left.\begin{aligned}\bar{\epsilon} &= 15\nu\overline{\left(\frac{\partial u}{\partial x}\right)^2} = \frac{15\nu}{2}\overline{\left(\frac{\partial w}{\partial x}\right)^2},\\ \overline{\chi_\theta} &= 6\mathscr{D}_\theta\overline{\left(\frac{\partial\theta}{\partial x}\right)^2}.\end{aligned}\right\} \tag{10}$$

Also, local isotropy implies that the structure functions of temperature of order p,

$$D_\theta^p(\Delta\xi) = \overline{[\theta(\mathbf{x}+\Delta\xi)-\theta(\mathbf{x})]^p} \quad (\xi = x, y, z), \tag{11}$$

have equal values for small separations in any of the three directions, if p is even, and are equal to zero if p is odd:

$$D_\theta^{2n}(\Delta x) = D_\theta^{2n}(\Delta y) = D_\theta^{2n}(\Delta z) \quad (\Delta x = \Delta y = \Delta z), \tag{12}$$

$$D_\theta^{2n+1}(\Delta x) = D_\theta^{2n+1}(\Delta y) = D_\theta^{2n+1}(\Delta z) = 0. \tag{13}$$

The 'transverse' structure functions of the velocity components, for small separations, should obey relations of the type:

$$D_u^{2n}(\Delta y) = D_w^{2n}(\Delta x) \quad (\Delta x = \Delta y), \tag{14}$$

$$D_u^{2n+1}(\Delta x) = D_u^{2n+1}(\Delta y) = D_w^{2n+1}(\Delta x) = 0. \tag{15}$$

Similar relations can be derived for the values of the autocorrelation functions, defined by

$$r_{\alpha,\alpha}(\Delta\xi) = \overline{\alpha(\mathbf{x}+\Delta\xi)\,\alpha(\mathbf{x})}, \tag{16}$$

for small separations, e.g.

$$r_{\theta,\theta}(\Delta x) = r_{\theta,\theta}(\Delta y) = r_{\theta,\theta}(\Delta z), \tag{17}$$

$$r_{u,u}(\Delta y) = r_{w,w}(\Delta x) = \left(1+\tfrac{1}{2}r\frac{\partial}{\partial r}\right)r_{u,u}(\Delta x), \tag{18}$$

for $\Delta x = \Delta y = \Delta z$.

From (18) one can derive an isotropic relation between the spectra of the cross-stream and longitudinal velocity components for the high wavenumbers k_1:

$$E_2(k_1) = E_3(k_1) = \frac{1}{2}\left(1 - k_1 \frac{\partial}{\partial k_1}\right) E_1(k_1), \tag{19}$$

with $\int_0^\infty E_i(k_1)\,dk_1 = \overline{u_i'^2}$, where u_i' is the fluctuating part of the velocity component u_i ($u_i = \bar{u}_i + u_i'$). From (19) it follows that, if $E_1(k_1)$ obeys a power law k_1^n, the transverse spectra obey the same power law with a constant ratio $E_3(k_1)/E_1(k_1) = \frac{1}{2}(1-n)$. This ratio is equal to $\frac{4}{3}$ in the case of the $-\frac{5}{3}$ law in Kolmogorov's (1941) inertial subrange.

In an isotropic flow the stress cospectrum $E_{1,3}(k_1)$, defined by

$$\int_0^\infty E_{1,3}(k_1)\,dk_1 = -\overline{u'w'},$$

is identically zero. So, local isotropy can also be tested by estimating the 'correlation-coefficient spectrum' or 'normalized-stress cospectrum'

$$R_{1,3}(k_1) = E_{1,3}(k_1)\,\{E_1(k_1)\,E_3(k_1)\}^{-\frac{1}{2}}, \tag{20}$$

which should roll off at high wavenumbers.

3. Experimental evidence for the velocity field

3.1. *Dissipative range*

According to Monin & Yaglom (1975), Townsend (1948) verified first the relations (1) in a macroscopically anisotropic turbulence, the wake behind a circular cylinder and, with a lesser degree of agreement, in a turbulent boundary layer over a flat plate (Townsend 1951).

Champagne, Harris & Corrsin (1970) estimated, in a nearly homogeneous tunnel flow, the lateral Taylor microscales from the spatial correlation coefficient functions

$$R_{\alpha,\alpha}(\Delta\xi) = \frac{r_{\alpha,\alpha}(\Delta\xi)}{\overline{\alpha'^2}} \tag{21}$$

of the transverse velocity components, with the help of the isotropic relation

$$\lambda_\xi^2 = -2 \Big/ \left\{\frac{\partial^2}{\partial \Delta\xi^2} R_{u,u}(\Delta\xi)\right\}_{\Delta\xi \to 0} \tag{22}$$

They compared these estimates with the longitudinal Taylor microscales λ_x obtained with the help of (4). They found that (1) and (5) were quite well verified, although (2) was clearly not. Champagne (1978) also reports a good verification of (1) in the wake of a cylinder.

The relation between the velocity-component spectra (19) was well verified in the dissipative range of scales by Gibson (1962, 1963) in a jet, Uberoi & Freymuth (1969, 1970) in cylinder and sphere wakes, and by Champagne (1978) in his nearly homogeneous flow and in a cylinder wake.

It is nevertheless interesting to note Uberoi's (1957) results on gradients and vorticity in a homogeneous flow and a boundary-layer shear flow. In the latter, he did not find any evidence of local isotropy, and the discrepancy between his results and (1) seemed to increase with the rate of deformation of the fluid.

Champagne (1978) also measured gradients and high-frequency spectra in an

axisymmetric free jet with a relatively high turbulence Reynolds number, $R_\lambda = (\overline{u'^2})^{\frac{1}{2}} \lambda_y/\nu \approx 626$. The gradients disagreed with (1) and the spectra with (19), at all scales. Yet we must note that, in this jet, the turbulence intensity was very high ($(\overline{u'^2})^{\frac{1}{2}}/\overline{U} \approx 0{\cdot}30$), so that Taylor's 'frozen-field' approximation was not valid. Champagne corrected his moments and spectra on the basis of Lumley's (1965) first-order model. But the corrections were so large that doubts remain on the validity of the corrected results, particularly since there has never been any experimental verification of Lumley's approximation.

The behaviour of the 'normalized-stress cospectrum' (20) has been observed by Corrsin (1949) and Tani & Kobayashi (1952) in jets, Laufer (1951) in a channel flow, Klebanoff (1953) in a boundary layer over a flat plate, and others. All results are similar to those of Champagne *et al.* (1970) in the homogeneous flow: after values of large amplitudes (of the order of 0·4) at low wavenumbers, $R_{1,3}(k_1)$ falls abruptly to negligible values at intermediate wavenumbers and in the dissipation range. Yet this behaviour does not seem to be a stringent test of local isotropy, as the range of k_1 where $R_{1,3}(k_1) \approx 0$ seems to extend to wavenumbers where other criteria of isotropy cannot be verified.

As a provisional conclusion, it appears that numerous results indicate that local isotropy seems verified in the dissipative range. There are only few results conflicting with the hypothesis; but, also, few experiments verified several of the consequences of the hypothesis.

3.2. *Inertial subrange*

A very large number of authors have reported measurements of approximate power laws in supposed inertial subranges, spectra proportional to $k_1^{-\frac{5}{3}}$ or second-order structure functions proportional to $\Delta x^{\frac{2}{3}}$. It has been said many times that these results prove the validity of the local isotropy hypothesis. Yet Champagne *et al.* (1970) had already observed that their spectra followed $k_1^{-\frac{5}{3}}$ laws although other criteria excluded the existence in their flow ($R_\lambda \approx 130$) of a range of scales intermediate between the production and the dissipation ranges where isotropic properties may be observed. They concluded that 'the Kolmogorov $-\frac{5}{3}$ law, even with proper component spectral magnitudes, is a relatively insensitive indication of local isotropy'. In fact, it is perhaps not even that.

Mestayer *et al.* (1976) pointed out that the spectra obtained in the atmosphere by several authors did exhibit large $-\frac{5}{3}$ ranges without agreeing with (19) in these ranges. Champagne (1978) noted that a large number of laboratory spectra present the $-\frac{5}{3}$ law shape far into ranges where other criteria (Corrsin 1958; Bradshaw 1969) clearly indicate that the flow cannot be isotropic. This point was actually mentioned by Monin & Yaglom (1975): they showed that the one-dimensional lateral-spectrum five-thirds law 'extends considerably further into the region of small wavenumbers than the subrange [of k_1] for which the five-thirds law is valid for the three-dimensional spectrum', and that the longitudinal-spectrum five-thirds law extends even further. So, even in the large-Reynolds-number geophysical flows, the extent of local isotropy should rather be deduced from the estimation of the ratio of the vertical- or transverse-velocity-component spectrum to the streamwise-velocity spectrum than from the width of the range of the approximate five-thirds law.

Schmitt, Friehe & Gibson (1978*a*) made a review of experimental estimates of the ratio $E_w(N)/E_u(N)$ obtained over land and sea (N is frequency). It appears that, as a general rule, the isotropic value of the ratio, $\frac{4}{3}$, is not attained. The only exceptions are the measurements made with a bivane–cup anemometer by Garratt (1972) and with sonic anemometers by Kaimal *et al.* (1972), Leavitt (1975),

Champagne *et al.* (1977). But, although the sonic anemometers have proved many times to be most valuable for measurements in the atmosphere, it seems to us that they are not to be trusted with regard to the $\frac{4}{3}$ ratio.

The first point to consider is that, in all cases where the $\frac{4}{3}$ ratio was reported, this value was attained by $E_w(N)/E_u(N)$ only for the highest frequencies that the sonic anemometers can measure, i.e at best the lowest frequencies of the inertial subrange. Interesting examples are given by the 1968 Kansas Experiment results. Kaimal *et al.* (1972) reported the results of the measurements with the sonic anemometers for various conditions of stability, the parameter z/L varying from -2 to $+1$. In unstable conditions the curves of $E_w(N)/E_u(N)$ attained values close to $\frac{4}{3}$ since $f = Nz/\overline{U} \approx 2$; in moderately stable conditions they seemed to tend towards $\frac{4}{3}$, but did not attain it at the highest frequency displayed, $f_i \approx 10$. During the Kansas Experiment, Larsen & Busch (1974, 1976) obtained high-frequency turbulent fluctuations by means of hot and cold wires mounted on a fast-responding vane placed at the 5·7 m level close to the Air Force Cambridge Research Laboratories instrumentation. It appears in the detailed analysis of Busch (1973) that the measurements of $E_w(N)/E_u(N)$ with the X-wire anemometers attained $\frac{4}{3}$, *on average* and with a dispersion of $\pm 15\,\%$, only for reduced frequencies f larger than 20; i.e. far into the $-\frac{5}{3}$ range of the spectra of w and u and for frequencies much greater than those the sonic anemometers can measure. Busch supposed these differences to be due either to the fact that Kaimal *et al.* (1972) included spectra from greater heights or to the 'arbitrary judgement involved'. We think that it could be due to a fault in the sonic-anemometer response.

We did not find in the literature direct comparisons of the frequency responses of sonic anemometers and of high-frequency probes as hot films or wires. McBean & Elliott (1978) measured simultaneously the static pressure and the velocity components with hot-wire and sonic anemometers. The cospectra of $\partial p/\partial t$ and u_{H} (hot-wire) on the one hand, and u_{S} (sonic) on the other hand, clearly indicate an attenuation in the sonic response above at least the reduced frequency $f = 0{\cdot}1$.

The author of the present paper was involved in two programmes where sonic and hot-film/wire anemometers were operated simultaneously. In both cases the anemometers were calibrated independently.

The experimental details of the participation of the University of California San Diego turbulence group to the GARP program AMTEX II have been described by Mestayer *et al.* (1978). The instruments were a three-way E. G. & G. Model 198 sonic anemometer and a 25 μm hot-film constant-resistance anemometer. The computation of the spectral coherency of the two output signals (after all due corrections) indicates a loss of coherency above 0·5–1 Hz; but this could be due to the distance between the two probes. Figure 1 compares the two spectra of the longitudinal velocity component multipled by N^2, where the frequency N is in hertz ($Nz/\overline{U} = 0{\cdot}92N$). With a path length p of 20 cm, the sonic anemometer was expected to measure frequencies up to $\overline{U}/2\pi p = 9$ Hz at least. On figure 1 one can observe at low frequencies the attenuation of the hot-film signal due to the lateral-component sensitivity of this probe. Note that the coherency is nevertheless very close to 1 in this range of frequencies. But on the high-frequency side the sonic clearly attenuates above 1–2 Hz.

In the ME . MO . MI . II experiment (Mestayer *et al.* 1980) the two-way E. G. & G. sonic anemometer of the group from the Observatoire du Pic du Midi was set at a distance of 1 m from the I.M.S.T. four-wire probe (Mestayer & Chambaud 1979). Although the sonic measured up to 30 Hz its effective cutoff frequency $\overline{U}/2\pi p$ was

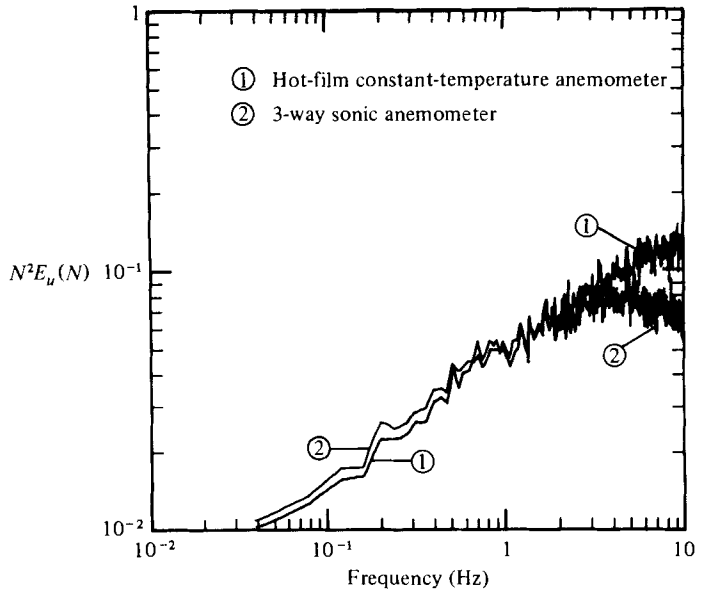

FIGURE 1. Spectrum of u' measured with a 3-way sonic anemometer and a hot-film anemometer (AMTEX experiment).

3–5 Hz, owing to the low mean velocity ($Nz/U = 1{\cdot}9N$). The comparison of the two spectra of u (figure 2) shows behaviour closely similar to those of the AMTEX experiment. The sonic anemometer appears to attenuate above 1–2 Hz. Finally, figure 3 compares the ratio $E_w(N)/E_u(N)$ obtained with the two anemometers. It is clear that, in the range 0·1–10 Hz, the ratios differ, although the u-spectra (figure 2), and also the w-spectra, are hardly discernible. Where the sonic data oscillate around $\frac{4}{3}$, the ratio obtained with the wire probe is around 1·1. These results, along with those of McBean & Elliott (1978) and Busch (1973), cast serious doubts on the validity of the $\frac{4}{3}$ ratios obtained with sonic anemometers. This attenuation could be due to wakes of the transducers along the acoustic path (Wyngaard 1981).

Nearly all measurements with X-wire anemometers yielded values of E_w/E_u lower than $\frac{4}{3}$ in the inertial subrange (Dunckel *et al.* 1974; Dreyer 1974; Revault D'Allonnes 1978; Schmitt *et al.* 1978*a*). Only Revault d'Allonnes and Schmitt *et al.* reported individual curves of $E_w(N)/E_u(N)$ versus N. They show behaviour closely similar to our curve of figure 3: oscillations around 1·1 in the inertial subrange and an increase over $\frac{4}{3}$ for the frequencies at the boundary between the inertial and dissipative ranges, as predicted by Wyngaard (1968). This seems to prove that local isotropy is verified only by the smallest scales, in the dissipative range, and that the $-\frac{5}{3}$ law is not closely related to isotropy.

4. Scalar-field experimental data

4.1. *Inertio-convective subrange*

There are few data available relating to the local isotropy assumption for the passive scalar contaminants in high-Reynolds-number turbulent flows.

Numerous authors have reported spectra of temperature, humidity, refractive index, and even particle or salt concentrations, measured in the atmosphere or large laboratory flows, that presented in the 'inertio-convective range' an approximate $-\frac{5}{3}$ power law. There is no reason to expect that the $-\frac{5}{3}$ law of scalar spectra is more

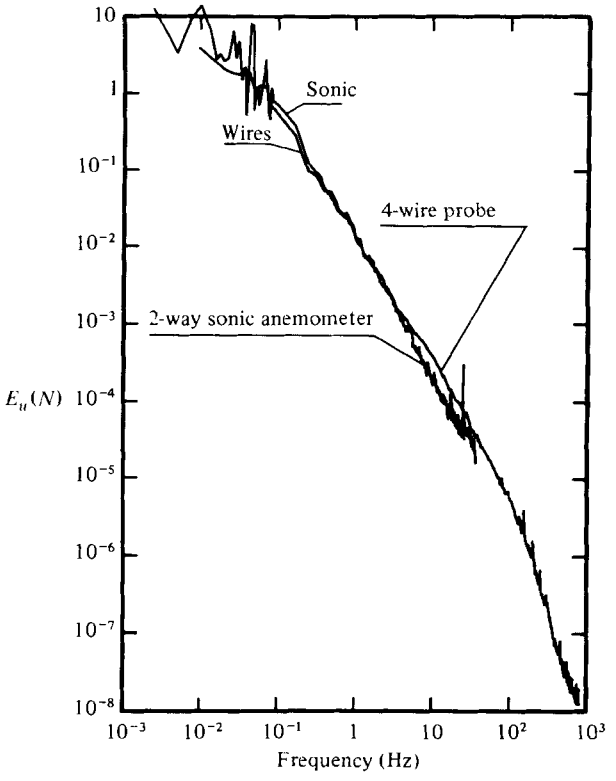

FIGURE 2. Spectrum of u' measured with a 2-way sonic anemometer and hot-wire anemometers (MEMOMI experiment).

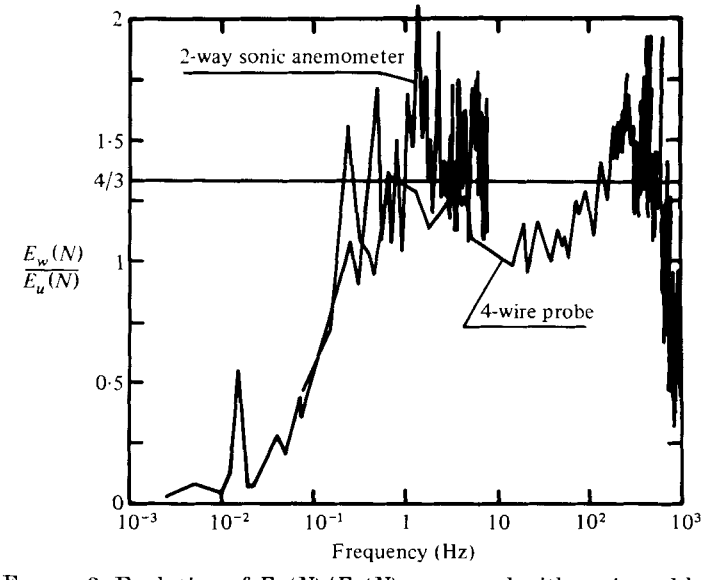

FIGURE 3. Evolution of $E_w(N)/E_u(N)$, measured with sonic and hot-wire anemometers (MEMOMI experiment).

closely related to the local isotropy of scalar fields than that of the velocity component spectra to the local isotropy of the turbulent dynamic field. However, in Obukhov's (1946) law expressed by

$$E_\theta(k_1) = \beta_\theta\, \bar{\epsilon}^{-\frac{1}{3}} \overline{\chi_\theta}\, k_1^{-\frac{5}{3}} \tag{23}$$

the constant β_θ should be universal. But there is such a large dispersion in the experimental estimates of β_θ, from 0·35 (Gibson & Schwarz 1963) to 1·17 (Gibson, Stegen & Williams 1970) that *universality* does not seem to hold. Note that these values of β_θ are related to the definition of $\overline{\chi_\theta}$ given by (9); some experimenters, defining $\overline{\chi_\theta}$ as the dissipation rate of $\frac{1}{2}\overline{\theta'^2}$, introduce constants twice as large. Note also that experimenters using (23) to estimate $\overline{\chi_\theta}$, generally choose β_θ between 0·4 and 0·5, but there is no experimental evidence for a unique value of β_θ.

On the contrary, without even considering the measurements made over the sea that may have been contaminated by salt spray (Schmitt, Friehe & Gibson 1978*b*), the fine spectra obtained with miniature platinum resistance thermometers (Champagne *et al.* 1977; Williams & Paulson 1978; Antonia *et al.* 1979; Mestayer *et al.* 1980) appear to present a behaviour slightly but clearly different from the $k_1^{-\frac{5}{3}}$ law. This difference is more neatly seen when the spectra are displayed multiplied by $k_1^{-\frac{5}{3}}$ in a log–linear plot: they present an 'inertio-convective subrange', which is not flat, indicating a spectral decrease less steep than $k_1^{-\frac{5}{3}}$. Williams & Paulson (1978) gave two hypotheses to explain this apparent 'bump' in the *compensated* spectrum (i.e. the spectrum multiplied by $k_1^{\frac{5}{3}}$): (i) the dissimilarities in the budget equations for the turbulent kinetic energy and temperature variance and in particular the role of pressure; and (ii) the beginning of a Batchelor's (1959) 'viscous–diffusive subrange' in k_1^{-1}, due to spatial dissimilarities in the fluctuations of the dissipations of kinetic energy and temperature variance (see the numerical simulations of Hill (1978) and Larchevêque *et al.* (1980)). This last hypothesis, implying a low correlation between the internal intermittencies of the dynamic and scalar fields, seems to contradict Obukhov's (1946) assumption that the scalar field local isotropy can be *naturally* deduced from the local isotropy of the dynamic field (but we must note that this contradiction does *not* imply by itself the local anisotropy of temperature).

Also, temperature structure functions of time $D_\theta^p(\Delta\tau) = \overline{\{\theta(t+\Delta\tau)-\theta(t)\}^p}$ were measured by Park (1976), Mestayer (1975), Antonia & Van Atta (1978) to estimate the longitudinal structure functions by assuming Taylor's hypothesis consequence $D_\theta^p(\Delta x) \sim D_\theta^p(\Delta\tau)$. The scatter of the results did not allow them to deduce much more from the even-order functions than from the spectra in the inertio-convective subrange. More significant is the clear departure of all odd-order functions from zero, which seems inconsistent with the isotropic relation (13), at least in this range of scales.

4.2. *Dissipative range*

As can be seen in the above relations (3)–(17), most direct verifications of the local isotropy assumption for scalar fields necessitate measurements at several points in space, which explains why there are so few available data. Freymuth & Uberoi (1971) verified relation (3) approximately in a heated wake, but found a value of $-0{\cdot}6$ for the skewness of the temperature derivative

$$S = \frac{\overline{(\partial\theta/\partial x)^3}}{[\overline{(\partial\theta/\partial x)^2}]^{\frac{3}{2}}}, \tag{24}$$

which should be zero, as are all odd-order moments of $\partial\theta/\partial x$, for an isotropic scalar field. A number of other authors measured $S(\theta) = \theta^3/(\theta^2)^{\frac{3}{2}}$ in various high-

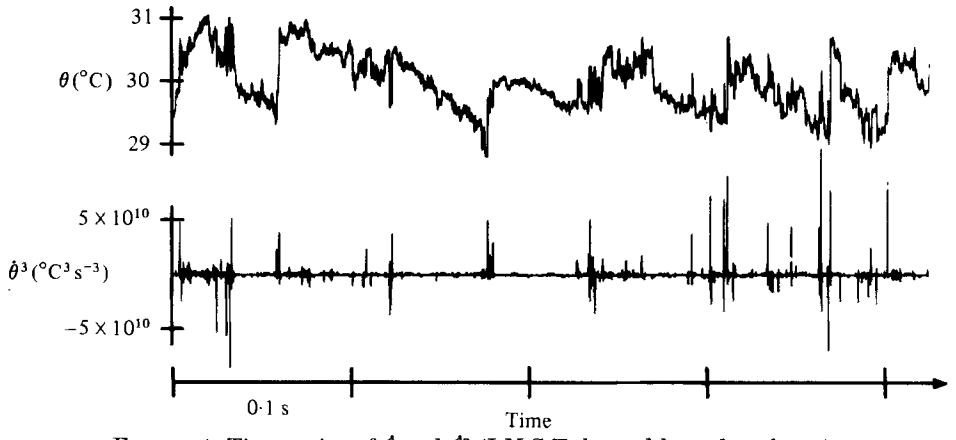

FIGURE 4. Time series of θ and $\dot{\theta}^3$ (I.M.S.T. heated boundary layer).

Reynolds-number flows where local isotropy was expected (see references in Sreenivasan & Tavoularis 1980). Most of them, assuming Taylor's hypothesis consequence $S(\dot{\theta}) = -S$, obtained also values of S of the order of unity. As the temperature derivative is known to be representative of only high wavenumbers, these results were considered to be in contradiction with the isotropy of small scales.

Mestayer *et al.* (1976) and Gibson, Friehe & McConnell (1977), after having proved that these non-zero values are not due to errors in temperature measurements with cold wires, showed that the sign of S is related to that of the mean temperature gradient. This observation led to the assumption that the small-scale anisotropy is connected to the large-scale structure of the flow: in particular, the sign of S and that of $\partial\bar{\theta}/\partial z$ change simultaneously with the direction of the large-scale ramps or sawtooth features that can be observed in the temperature signal and which seem to be characteristic of the sheared turbulent scalar fields (Gibson *et al.* 1977).

In a number of works (see references in Sreenivasan, Antonia & Britz 1979) the effects of the ramps and the characteristics of the *superimposed* small-scale fluctuations have been computed with a simplified sawtooth model (Antonia & Van Atta 1978, 1979) or measured in a heated jet with a signal-conditioning method (Sreenivasan *et al.* 1979). These studies tend to demonstrate that the experimental data that indicate the temperature anisotropy, i.e. non-zero odd-order time-dependent structure functions (Antonia & Van Atta 1978) and non-zero derivative skewnesses (Sreenivasan *et al.* 1979), are due mainly to the large-scale ramps, the sharp abrupt fronts of which contribute to some high-frequency characteristics, and that the *superimposed* small-scale fluctuations are nearly isotropic. In particular, in the heated axisymmetric jet of Sreenivasan *et al.* (1979) the *superimposed* signal is obtained by subtracting, in ramps of a definite length, the ensemble average of the ramps from the temperature signal. This new signal has a derivative skewness equal to only 0·33, instead of 0·87 for the original signal.

These studies assume that the *superimposed* small-scale fluctuations are uncorrelated with the ramps, that the fronts of these are always sharp and extremely thin, and that the ramps are present everywhere in the signal, quasi-regular and contiguous. Figure 4 presents simultaneous time traces of θ and $\dot{\theta}^3 = (\partial\theta/\partial t)^3$ obtained in the heated boundary layer of the IMST tunnel ($\partial\bar{U}/\partial z \approx 4\ \mathrm{s}^{-1}$; $\partial\bar{\theta}/\partial z \approx +5\ ^\circ\mathrm{C/m}$). It is obvious that the sharp fronts of the ramps provide positive contributions to $\dot{\theta}^3$ (here $S(\partial\theta/\partial x) = -S(\dot{\theta}) = -0{\cdot}63$). But it is also clear that the ramps are very irregular, not as sawtooth-like as in the heated-jet signal of Sreenivasan *et al.* (1979), not

contiguous but altogether overlapping and/or disjointed, with large periods of fluctuating signal belonging to no ramp (this is not taken into account in the analysis of Sreenivasan *et al.*). This figure also shows that the use of a very small probe of length equal to η allows the observation of a structure of front regions more complex than was suspected previously. Nevertheless, it could be of interest to adapt conditional measurements to flows with no external intermittency, such as heated homogeneous shear flows or boundary layers at $z/\delta < 0{\cdot}4$.

Sreenivasan & Tavoularis (1980) have shown that the existence of a non-zero skewness and its sign are connected to the presence of both velocity and temperature mean gradients. Yet it is still not clear why the values of S keep the same magnitude when the Reynolds number of the flow increases, i.e. when the relative frequency of ramp fronts decreases; this could be an indication that the ramps then become a more general feature of the signal, overlapping and superposing at large and smaller scales, 'maintaining' down to small scales the anisotropy of the macroscopic flow (Wyngaard 1976; Freymuth 1981).

Temperature spatial gradients have been measured by Sreenivasan, Antonia & Danh (1977) in a small laboratory heated boundary layer and by Antonia *et al.* (1979) in the atmospheric surface layer, providing data for direct tests of the local isotropy assumption (by *direct* we mean that in those tests there is no need for Taylor's hypothesis to be verified). As interpreted by Van Atta (1977) the derivative spectra obtained in the laboratory ($R_\lambda \approx 150$) indicate a rather good agreement with the hypothesis of local isotropy, in the dissipative range, in the streamwise and transverse direction, along with a clear disagreement in the vertical direction. The atmospheric data are not clearly conclusive, apparently because of the errors due to the so-called *gradient probes* (Mestayer & Chambaud 1979) and to the use of Taylor's hypothesis to estimate $\partial u/\partial x$.

5. Technical arrangements and signal processing

The measurements described in this paper were made in the I.M.S.T. Air–Sea Interaction Tunnel (Coantic *et al.* 1969), in the heated air flow over the water surface. The boundary layer, developed over 34 m, has a thickness δ of 0·75 m in the measurement section and is 3 m wide. The mean wind speed, $U_\infty = 8{\cdot}9$ m/s, the mean temperature θ_∞ outside the boundary layer, and the surface temperature θ_s ($\theta_\infty - \theta_s \approx +10{\cdot}7$ °C) were controlled with accuracies of 0·01 m/s and 0·1 °C and measured during all the experiments with a miniature Pitot tube connected to a precision M.K.S. Baratron electrical manometer and with thin thermocouples. The probes were located in the median plane of the test section at an elevation $z = 0{\cdot}25$ m over the water surface. The experimental conditions and the values of the various parameters characterizing the turbulent field are presented in table 1.

Two sets of measurements were made. First, a DISA 55 P 11 X-wire probe made of two 1·25 mm long slanted tungsten wires (5 μm in diameter) separated by 1·25 mm was combined with a 1·25 mm long straight wire and a 0·3 mm long Wollaston cold wire with a diameter of 0·635 μm, in a 2·5 mm wide multiwire probe to measure simultaneously u', w' and θ' (Mestayer 1980). In the second set of measurements, two identical cold wires measured θ' simultaneously at two points in space separated by a distance varying between 1 mm and 20 cm either in the longitudinal direction x parallel to $\overline{U}$, or in the transverse horizontal direction y. Measurements of u' have also been made with two hot wires separated in the transverse direction. The probe separations were known to an accuracy of 5 μm.

$$\frac{z}{\delta} = 0{\cdot}33 \quad \overline{U} = 7{\cdot}5 \text{ m s}^{-1} \quad \overline{\theta} = 23{\cdot}8\ ^{\circ}\text{C} \quad \theta_s = 15{\cdot}0\ ^{\circ}\text{C}$$

$$\frac{\partial \overline{U}}{\partial z} = 4{\cdot}0 \text{ s}^{-1} \quad \frac{\partial \overline{\theta}}{\partial z} = 4{\cdot}8\ ^{\circ}\text{C m}^{-1}$$

$$(\overline{u'^2})^{\frac{1}{2}} = 0{\cdot}70 \text{ m s}^{-1} \quad (\overline{w'^2})^{\frac{1}{2}} = 0{\cdot}54 \text{ m s}^{-1} \quad (\overline{\theta'^2})^{\frac{1}{2}} = 0{\cdot}49\ ^{\circ}\text{C}$$

$$\bar{\varepsilon} = 0{\cdot}635 \text{ m}^2 \text{ s}^{-3} \quad \eta = 0{\cdot}27 \times 10^{-3} \text{ m} \quad \lambda = 0{\cdot}013 \text{ m} \quad R_\lambda = 616$$

Table 1. Experimental conditions

The technical set-up of the probes and design of the probe holders were fully described by Mestayer & Chambaud (1979), along with the calibration techniques, the choices of the operating parameters and the performance of the apparatus. The cold wires were operated in DISA 55 M 20 constant-current 1 : 20 bridges and the hot wires in matched DISA 55 M 10 constant-resistance bridges. The cold-wire operating current was set to 0·6 mA when operated in the multiwire probe, which resulted in a time constant smaller than 15 μs and a sensitivity ratio $r_s = (\partial e/\partial u)/(\partial e/\partial \theta) \approx 0{\cdot}036$, taken into account in the data-reduction procedure described below. For the measurements with the isolated cold wires, i.e. the measurements at two space points, the current was 0·2 mA and the effect of the small velocity sensitivity ($r_s \approx 8 \times 10^{-3}$) has been shown to be negligible in the range of separations which we are interested in. Figure 5 shows a preliminary test of this effect: the temperature autocorrelation coefficient function $R_{\theta\theta}(\Delta\tau) = \overline{\theta'(t+\Delta\tau)\,\theta'(t)}/\overline{\theta'^2}$ has been computed for five successive measurements with various currents I. The effect of the sensitivity to velocity fluctuations, which increases with the current, is seen to be non-negligible for the large time lags but extremely small for the small time lags (upper curves); actually it is even smaller for $I = 0{\cdot}2$ mA.

All spectra presented here were obtained from the multiwire-probe measurements. The four wires had been calibrated for velocity amplitude, velocity direction and temperature. The signals from the four wires were simultaneously low-pass filtered, sampled and digitized. The sets of four digital data were processed together (using, for the hot wires, response laws derived from the results of Champagne, Sleicher & Wehrmann (1967)) to separate the time series proportional to u', w' and θ', corrected for any parasitic contamination (Mestayer 1982).

Figure 6 presents the further stages of data processing. The dots (*a*) are the spectral estimates obtained with a fast-Fourier-transform routine from three successive recordings sampled at the rates of 10000, 2500 and 312·5 samples/s (large arrows) and previously low-pass filtered with 21 db/octave analog filters at the frequencies indicated by the small arrows, to avoid the aliasing effect. Actually, the estimates of the higher-frequency band, where the slope of the spectrum is steep and rapidly changing, were obtained from the second-derivative spectrum (i.e. the signal was digitally differentiated twice before the fast-Fourier-transform computation and the estimates of $E_{\partial^2\theta/\partial t^2}(N)$ were then divided by $(2\pi N)^4$ to obtain the dots of the (*a*) curve. This 'pre-whitening' greatly improves the spectral estimation by reducing the 'leakage'. On the left of the (*a*) curve is indicated the value of the 99% confidence interval, which is identical for all estimates, as the three recordings consisted of the same number of samples (292 times 1024). At the high-frequency end of the (*a*) curve one can see small peaks at frequencies that are exact multiples of 50 Hz, which are due to unavoidable noise, electromagnetic waves picked up by the hot and cold wires themselves. In the 'cleaned' curve (*b*) they have been removed along with the

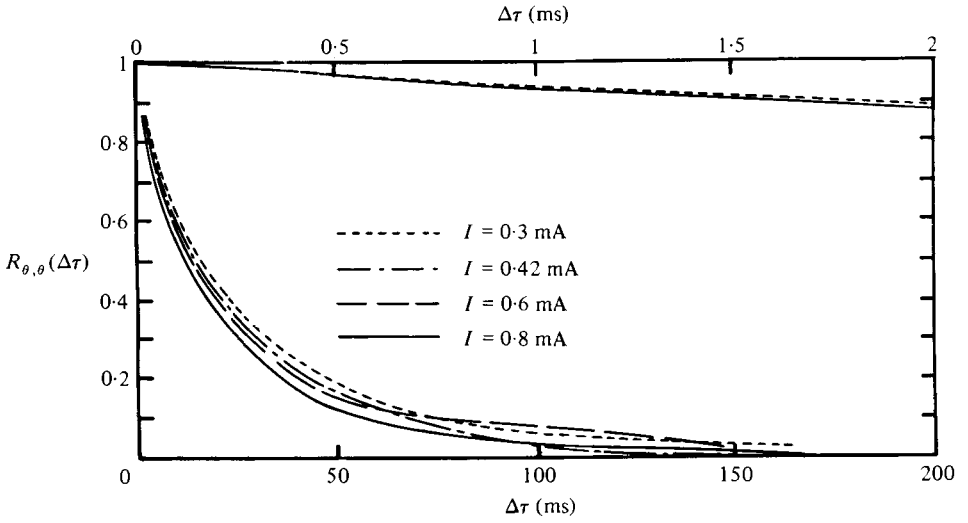

FIGURE 5. Autocorrelation-coefficient functions measured with various cold-wire currents (upper curves refer to the expanded upper scale).

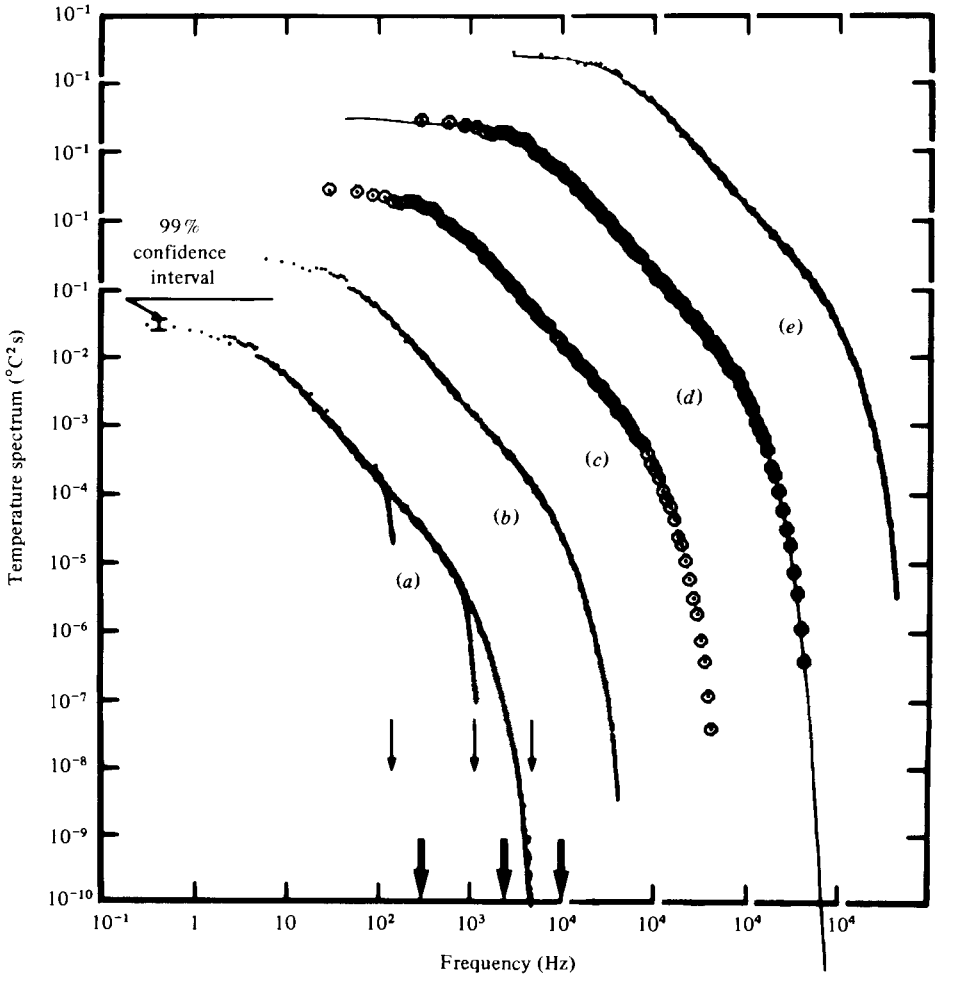

FIGURE 6. Stages in the process of obtaining the spectral curves.

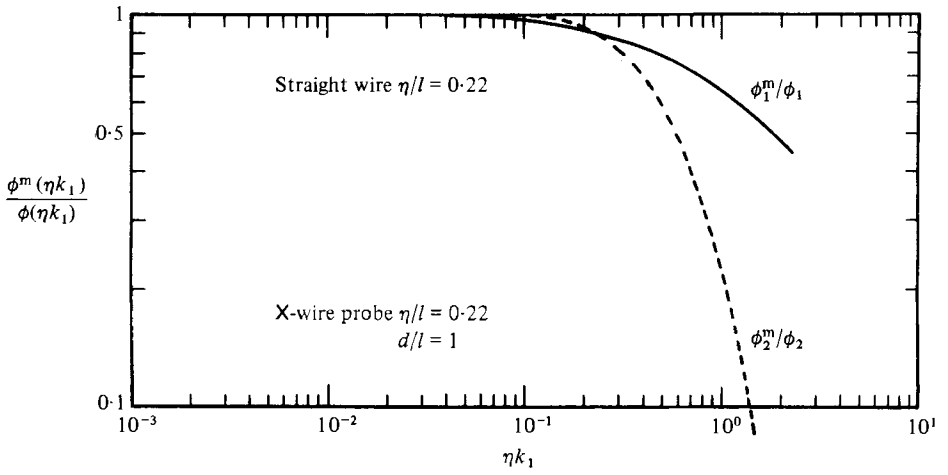

FIGURE 7. Attenuations due to the spatial resolution of probes.

estimates belonging to the 'roll-offs' due to the low-pass filterings at frequencies close to 0·8 times the Nyquist frequencies. The (*b*) estimates were then logarithmically 'cleared' by polynomial interpolations, (*c*). The curves that are presented here were then obtained by fitting eleventh-order Tchebycheff polynomials to the logarithms of these last estimates. On figure 6, the curve is compared in (*d*) with the 'cleared' estimates, and, in (*e*), with the 'cleaned' estimates, restricted to the range of frequencies effectively measured.

A last correction has been applied to the spectra of velocity components to take into account the high-frequency attenuation due to the spatial resolution of the hot wires. They had a length 4·5 times greater than Kolmogorov microscale. Their highest-frequency measurements can be interpreted as measurements of an integral of the field along their length. Wyngaard (1968) made a semi-theoretical study of this effect, based on the 'Pao's (1965) spectrum' model of the dissipative range. From Wyngaard's results, we computed the expected ratios of the measured ϕ^m to *true* ϕ spectra (figure 7). Those were used to correct our high-wavenumber spectra. It is worth noting that, although the probes are used all together in a 'multiwire probe', their spatial resolutions to measure the smallest scales remain those of the individual probes, because of the high value of the sensitivity ratio $(\partial e/\partial u)/(\partial e/\partial \theta)$ for the hot wires (≈ -80), and its small value for the cold wires ($\approx -0{\cdot}036$) (Mestayer 1982). Although there are serious doubts about the validity of Taylor's hypothesis, the wave-number functions were deduced from the frequency functions using the straight-forward relation $k_1 = 2\pi N/\overline{U}$, as Lumley's (1965) and Wyngaard & Clifford's (1977) studies indicated that the errors should be small, with $(\overline{u'^2})^{\frac{1}{2}}/\overline{U} \approx 0{\cdot}09$: smaller than 5 % for the u-spectrum and 3 % for the w-spectrum, at the highest wavenumbers.

To obtain the spatial correlation and structure functions, the measurements at two points have been reduced with a mixed analog–digital procedure. The signals were not digitized on-line but recorded on a Schlumberger MP 5522 f.m. analog tape recorder at 76 cm/s with a 51 db signal-to-noise ratio after analog filtering at 5000 Hz to remove noise. When played back, on each record the two signals were so amplified as to take into account the variations of the probe sensitivities and analog filtered: low-pass at 4400 Hz (Kolmogorov frequency $N_K = 4420$ Hz) and high-pass at 0·01 Hz to remove the small but cumbersome temperature trends of the tunnel thermal regulation. The data were sampled at a rate of 625 samples/s during 12 minutes, then

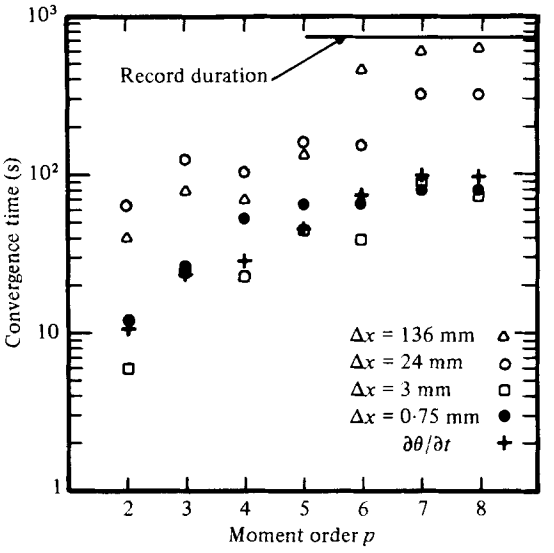

FIGURE 8. Times of convergence $\pm 5\%$ of the moments of $\Delta\theta = \theta(x+\Delta x)-\theta(x)$.

digitally recalibrated and centred around their means. The products and moments of the differences were computed and averaged by direct cumulative averaging to avoid all effects of digital filtering and rounding-up. Figure 8 shows that the record duration was always greater than the time necessary to obtain the final value $\pm 5\%$ of the moments $\langle(\Delta\theta)^p\rangle = D_\theta^p$ of the increments $\Delta\theta(\Delta x) = \theta(x+\Delta x)-\theta(x)$.

The measurements with two probes with a separation normal to the mean wind direction do not raise major problems, if the moving-probe displacement is accurate (Mestayer & Chambaud 1979) and if the distance between the probes remains large enough to avoid the effects of the thermal and dynamic wakes: the minimal admissible distance between two hot wires seems to be about 1 mm, and between two small cold wires, about 0·1 mm. But when the separation is in the mean-flow direction the problem increases considerably. The thermal and dynamic wakes of the hot wires are highly fluctuating and they survive for long distances: the longitudinal velocity functions have been found not to be directly measurable between 1 mm and 20 cm. As for the temperature measurements, Mestayer & Chambaud (1979) described the setting up of small wires allowing measurement of the longitudinal functions: the values of $\bar{\theta}$, $\overline{\theta'^2}$ and $E_\theta(N)$ measured at the various separations showed no discernible wake effect. Tests have also been made to examine the dynamic wake effects: one of the wires was replaced by a velocity wire either downstream or upstream of the other temperature wire. There is no discernible systematic trend in the mean-velocity value (figure 9) or in the value of $\overline{u'^2}$ for distances greater than 0·3 mm. Observation of the u' spectra show no deformation at any distance; except perhaps isolated over-contributions of only a few per cent located at frequencies that could be the first harmonics of the Strouhal frequencies of the wire and the prongs (Mestayer 1980): their effects on the temperature field are negligible.

6. Results for the dynamic field

Various criteria have been proposed to predict the existence of local isotropy and that of an inertial subrange. They are based on Kolmogorov's (1941, 1962) assumptions that this subrange exists when the wavenumber ranges of turbulent kinetic

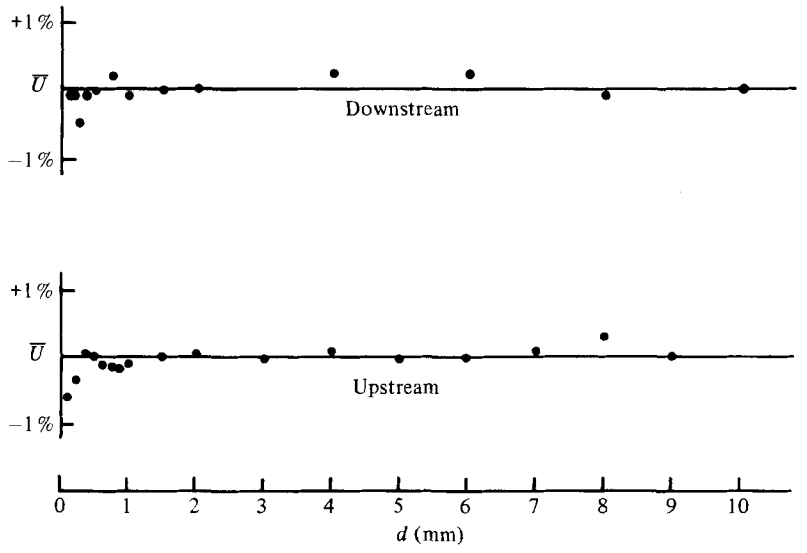

FIGURE 9. Measurements of the mean velocity downstream and upstream of a cold wire.

energy production and dissipation are separated. Corrsin (1958) proposed numerical relations between timescales representative of smaller and larger scales, $\eta/v_K = (\nu/\epsilon)^{\frac{1}{2}} \ll |\partial\overline{U}/\partial z|^{-1}$; or between the wave numbers representative of the dissipative range k_d ($\sim 0{\cdot}1k_K$) and of the production range $k_p \sim \overline{(u'^2)}^{-\frac{1}{2}}|\partial\overline{U}/\partial z|$, $k_d \gg k_p$. In the present experiment these criteria can be considered as largely met:

$$\left(\frac{\nu}{\epsilon}\right)^{\frac{1}{2}}\left|\frac{\partial\overline{U}}{\partial z}\right| = 0{\cdot}02, \quad 0{\cdot}1k_K\, k_p^{-1} = 65. \tag{25}$$

Actually, figure 10(*a*) shows that the production and dissipation spectra are neatly disjointed, but not separated by a large range where they would be altogether negligible, although the ratio of the wavenumbers of the peaks of the two spectra is 200, even larger than $0{\cdot}1k_K\, k_p^{-1}$.

Local isotropy could thus be expected, not only in the dissipative range but also in an intermediate 'inertial' subrange, say for $k_1\eta > 10^{-2}$.

Figure 10(*b*), where the spectra, normalized with Kolmogorov variables

$$\phi_i(\eta k_1) = (v_K^2\eta)^{-1}\, E_i(k_1) = \bar{\epsilon}^{-\frac{1}{4}}\nu^{-\frac{5}{4}}E_i(k_1) \quad (i = 1, 3), \tag{26}$$

$$\Gamma_\theta(\eta k_1) = \bar{\epsilon}^{\frac{3}{4}}\nu^{-\frac{5}{4}}\overline{\chi_\theta}^{1}E_\theta(k_1), \tag{27}$$

are multiplied by $(\eta k_1)^{\frac{5}{3}}$ to emphasize their behaviour in the intermediate range of wavenumbers, proves that this is not the case. The consequences of the spectral behaviours observed here will be studied and compared with previous results in a paper in preparation. We can note here that the spectra do not present exact $-\frac{5}{3}$ power laws that would appear here as plateaus, the values of which would be equal to Kolmogorov's 'universal constants' α_1, α_3 and β_θ. Anyhow, it is clear that the transverse spectrum computed from the measured longitudinal spectrum ϕ_1 with help of the isotropic relation (19) (dashed line) is not equal to the measured spectrum ϕ_3 for wavenumbers $k_1\eta$ smaller than 5×10^{-2}, i.e. in the expected inertial subrange. Nevertheless it is interesting to note the small plateau of ϕ_1 in the range $2\times10^{-3} < \eta k_1 < 10^{-2}$. It indicates a decrease of ϕ_1 proportional to $(\eta k_1)^{-\frac{5}{3}}$ in a region of wavenumbers where isotropy is not satisfied and where the production of turbulent

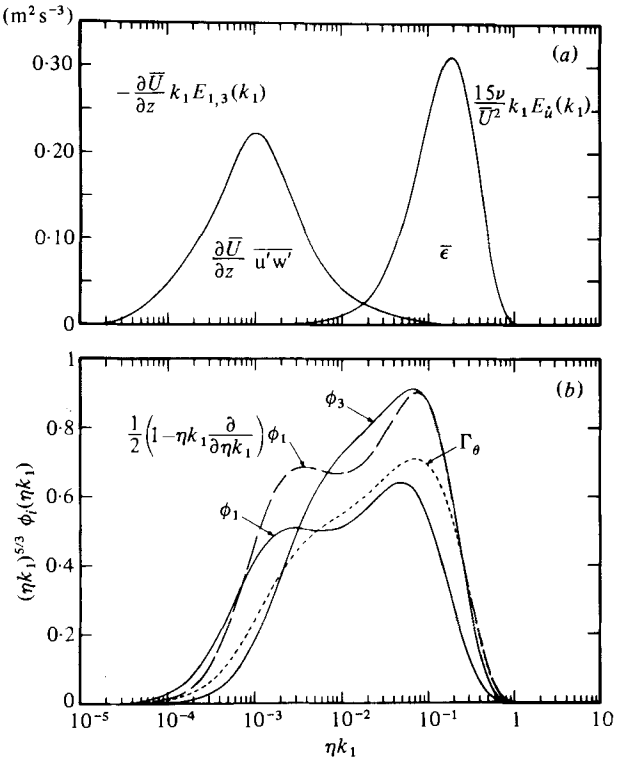

FIGURE 10. (*a*) Spectral contributions to the rates of turbulent kinetic energy production and dissipation. (*b*) 'Inertial' subrange spectra, in Kolmogorov scales: dotted and plain lines are the measured spectra; the dashed line is the transverse spectrum computed from ϕ_1 with help of the isotropic relation (19).

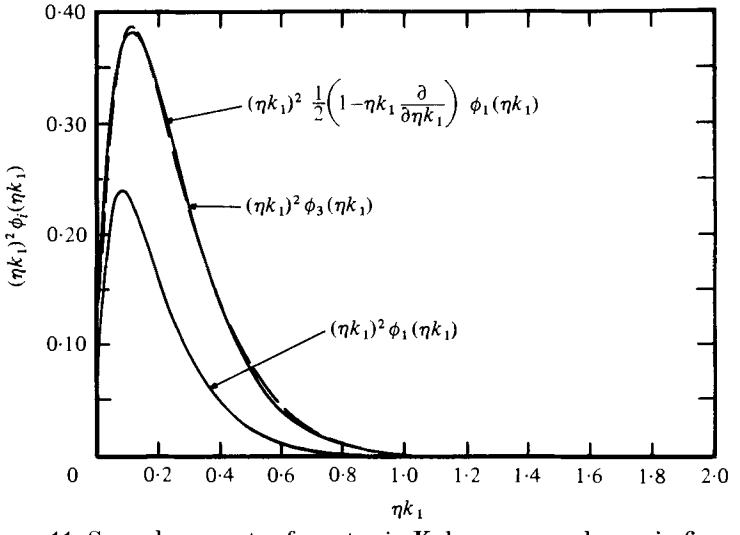

FIGURE 11. Second moments of spectra in Kolmogorov scales, as in figure 10(*b*).

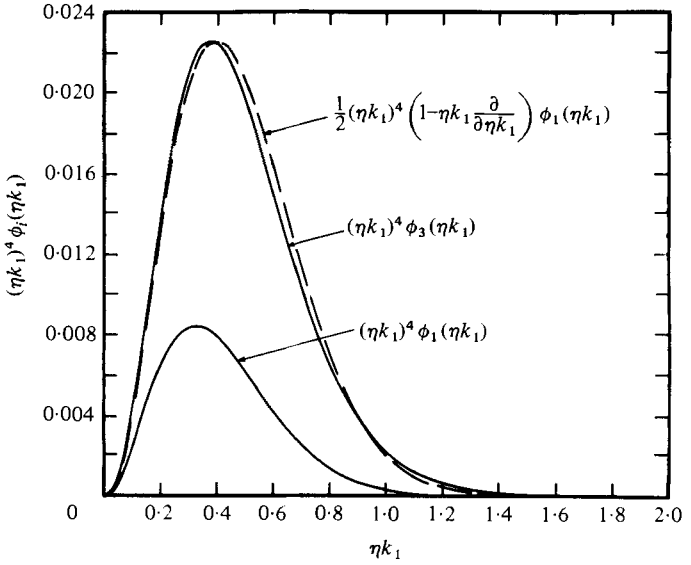

FIGURE 12. Fourth moments of spectra, as in figure 10(*b*).

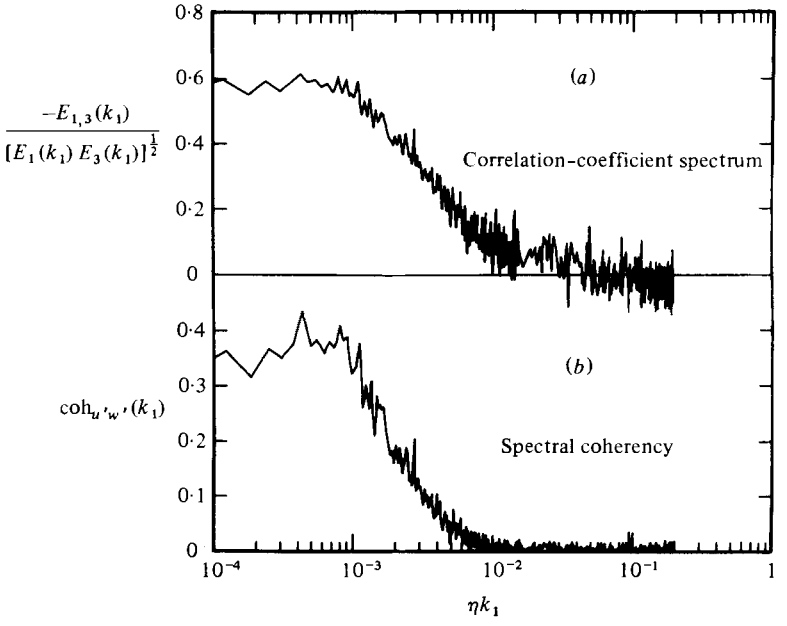

FIGURE 13. Correlation-coefficient spectrum and spectral coherency of the velocity components.

kinetic energy is not negligible (figure 10*a*), although one cannot consider it as an *extension* to smaller wavenumbers of any inertial subrange $-\frac{5}{3}$ law (see §3.2). For the higher wavenumbers up to $k_1\eta = 1$ and over, figures 11 and 12 present the second and fourth moments of the measured spectra ϕ_1 and ϕ_3 and of the computed transverse spectrum. They show that the relation (19) is satisfied with a very good approximation in the dissipative range.

The correlation-coefficient spectrum defined by (20) is displayed in figure 13 (*a*). The value of the correlation between u' and w' is high at low wavenumbers and falls to

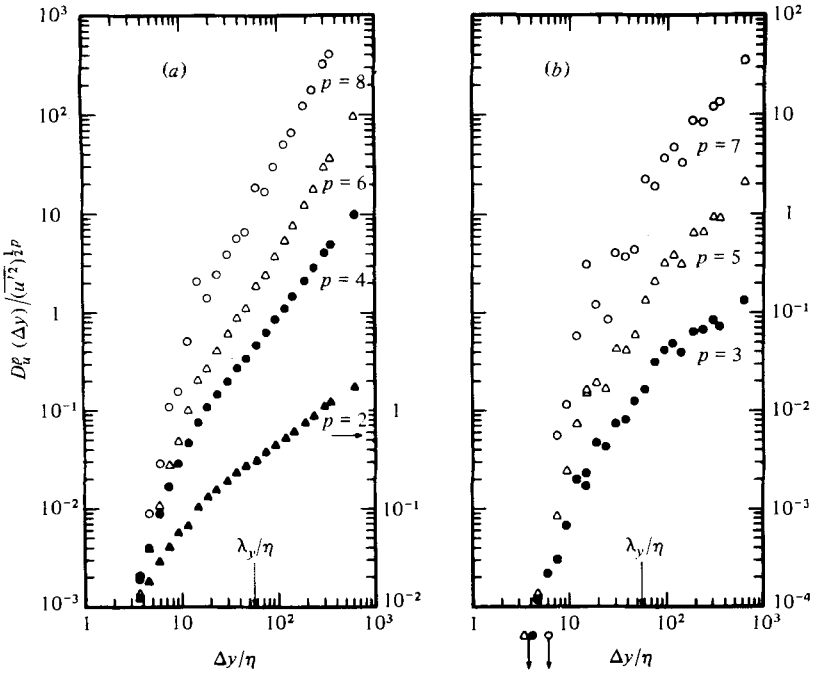

FIGURE 14. Even- and odd-order transverse structure functions of u'.

the isotropic value zero for wavenumbers $k_1\eta$ larger than 3×10^{-2} at most. The spectral coherency, or cross-spectrum modulus, defined by

$$[\mathrm{coh}_{u',w'}(k_1)] = [E^2_{1,3}(k_1)+\mathrm{Qu}^2_{1,3}(k_1)]\,[E_1(k_1)\,E_3(k_1)]^{-1}, \tag{28}$$

where $\mathrm{Qu}_{1,3}(k_1)$ is the quadspectrum of u' and w', is null in an isotropic field. Figure 13 (*b*) shows that it presents a high and nearly constant value at low wavenumbers and a relatively fast decrease to zero above $k_1\eta = 10^{-2}$. This indicates that zero coherency is a relatively weak test of local isotropy.

The transverse structure functions of u', presented normalized by $\overline{u'^2}$ in figure 14, result from the simultaneous measurements with two identical hot wires separated in the horizontal direction normal to the mean wind speed by distances varying from 1 mm to 20 cm. The even-order functions present expected behaviours: regular increases with $\Delta y/\eta$ and power laws in the intermediate range of separations (which will be discussed elsewhere). By comparison, the odd-order functions appear to have rather chaotic behaviours, the main feature of which seems to be the fast roll-off for distances $\Delta y/\eta$ smaller than 10 (the vertical arrows under the lower left corner of figure 14 (*b*) indicate that the functions change sign for the corresponding values of $\Delta y/\eta$).

By assuming that

$$D^p_w(\Delta\tau) \sim D^p_w(\Delta x), \tag{29}$$

the time-dependent structure functions of w' can also be regarded as estimates of the transverse functions, as w is in a direction normal to Δx. The even-order functions $D^p_w(\Delta\tau)$ of figure 15 have the same general regular behaviour as the transverse functions $D^p_u(\Delta y)$ of figure 14 (*a*), except for the smallest separations, for which the X-wire-probe resolution is insufficient, and for the largest separations, because the vertical fluctuations can hardly contribute to scales larger than the

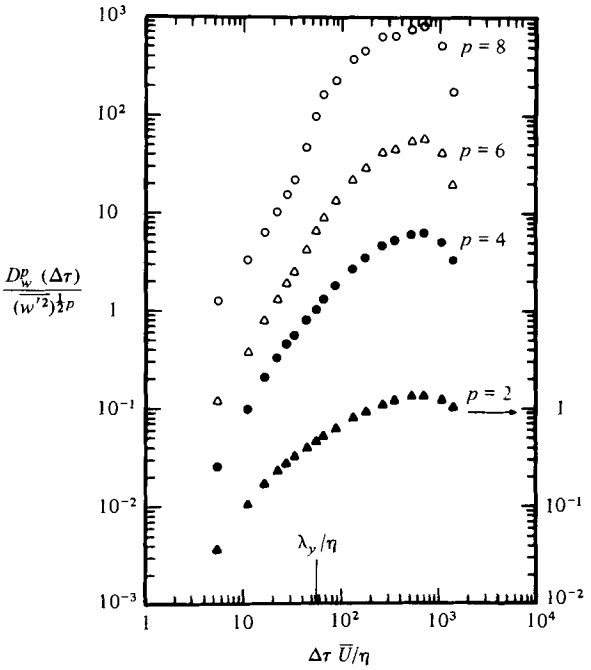

FIGURE 15. Even-order time-dependent structure functions of w'.

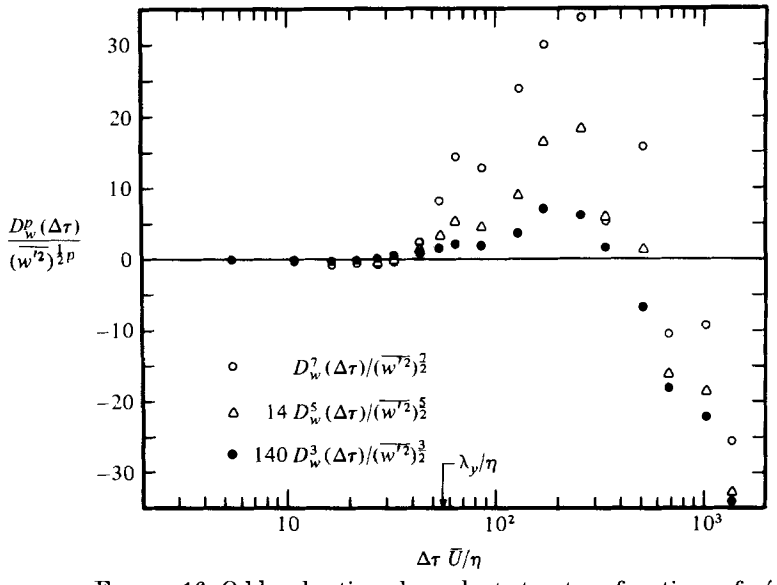

FIGURE 16. Odd-order time-dependent structure functions of w'.

boundary-layer thickness δ ($\delta/\eta \approx 2{\cdot}8 \times 10^3$). The odd-order functions $D_w^p(\Delta\tau)$ (figure 16) present very different behaviours, with two changes of sign around $\Delta\tau\overline{U}/\eta = 5 \times 10^2$ and for $\Delta\tau\overline{U}/\eta = 30$. For smaller separations these functions remain very close to zero, the isotropic value.

From the measurements with two hot wires we also obtained the transverse autocorrelation coefficient function of u'. A plot of the derivative of $R_{u,u}(\Delta y)$ with respect to Δy (figure 17, left and upper scales) allows us, by means of (22), to estimate

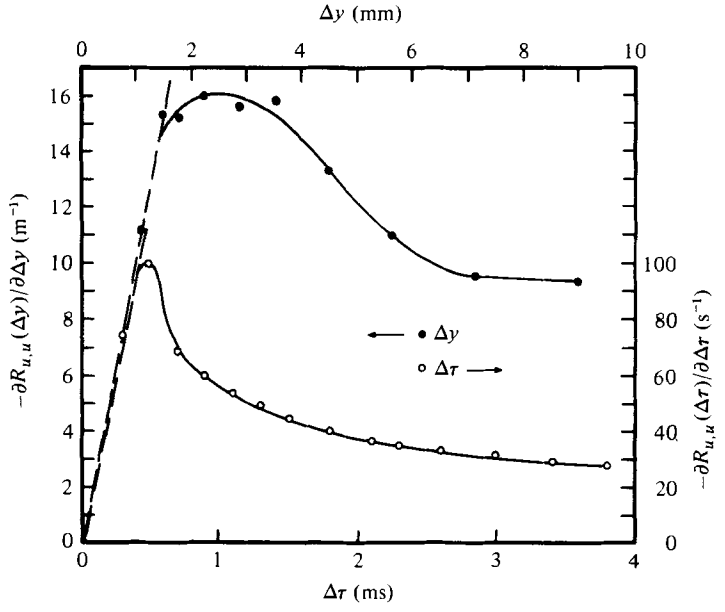

FIGURE 17. Derivatives of the transverse and time-dependent autocorrelation-coefficient functions of u'.

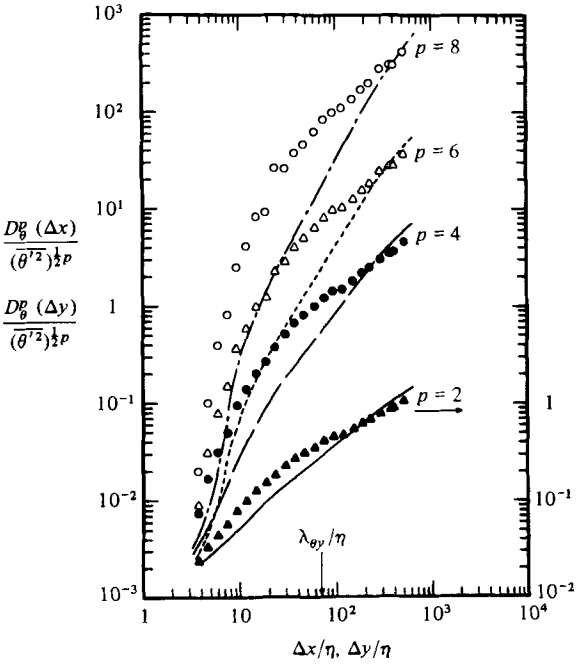

FIGURE 18. Longitudinal (symbols) and transverse (lines) temperature structure functions of even orders.

the transverse Taylor microscale: $\lambda_y \approx 1{\cdot}5 \times 10^{-2}$ m. Similarly the derivative of the time autocorrelation function $R_{u,u}(\Delta\tau)$ (right and lower scales in figure 17) lets us estimate the longitudinal Taylor microscale λ_x, with the help of Taylor's hypothesis

$$\lambda_x^2 \approx -2\overline{U}^2 \Big/ \left[\frac{\partial^2}{\partial \Delta\tau^2} R_{u,u}(\Delta\tau)\right]_{\Delta\tau \to 0}, \tag{30}$$

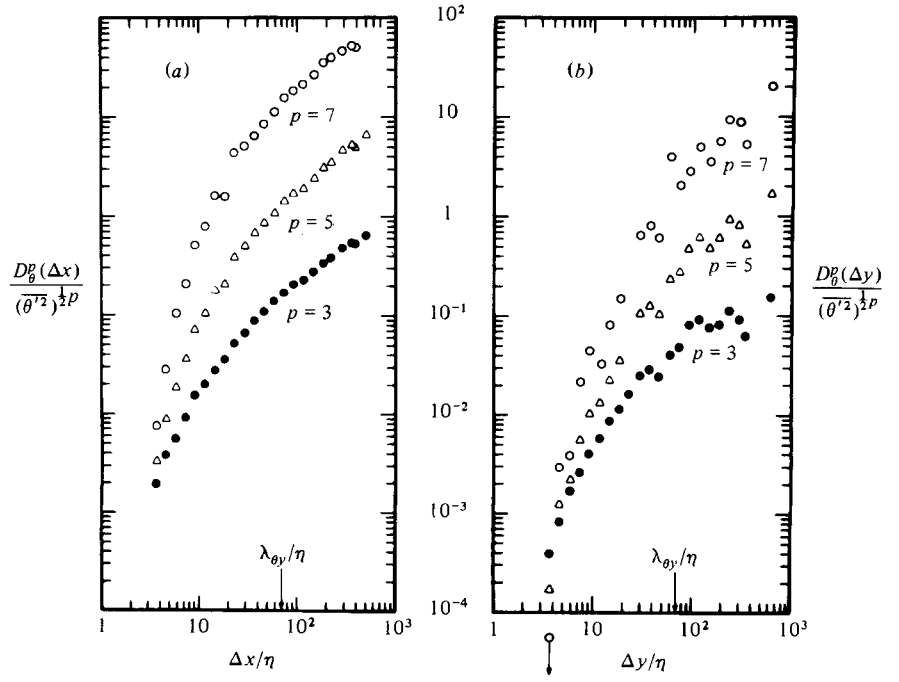

FIGURE 19. Longitudinal and transverse temperature structure functions of odd orders.

that is $\lambda_x \approx 2{\cdot}13 \times 10^{-2}$ m. The ratio λ_x/λ_y has the value 1·42, verifying well the isotropic relation (5).

These data provide an important set of converging evidence that the local-isotropy assumption is verified in the dissipative range of scales smaller than 20η: the ratio of the microscales deduced from the curvatures at the origin of the longitudinal and transverse autocorrelation functions of u', the falling to zero of the odd-order transverse structure functions $D_u^p(\Delta y)$ and $D_w^p(\Delta\tau)$ for small separations, the falling to zero of the correlation-coefficient spectrum and the spectral coherency of u' and w', and verification of the isotropic relation (19) by the longitudinal and vertical spectra for high wavenumbers. Although the zones where the spectral coherency $\mathrm{coh}_{u'w'}(k_1)$ and, to a lesser degree, the correlation-coefficient spectrum and the structure functions of w' are equal to zero extend to larger scales, the assumption does not seem to be verified for scales larger than 20η ($k_1\eta < 5 \times 10^{-2}$), conspicuously so for the scales at which a Kolmogorov inertial subrange could be expected.

It is worth noting that these results have been verified in other sets of measurements done in the tunnel, in particular when the mean temperature gradient was inverted.

7. Results for the temperature field

The most critical test of the assumption of local isotropy of the temperature field we have been able to realize is the direct comparison of the longitudinal and transverse structure functions and autocorrelation functions. Indeed, the two sets of measurements have been realized with the same probes, same sensitivities and precisions, and no additional assumption.

Isotropy implies the equality of the even-order temperature structure functions in all directions (equation (12)). The results of figure 18, where the symbols are the values of the longitudinal functions and the lines are the curves fitted to the measurements

of the transverse functions, show that the two sets of functions are not equal in any range of separations. If one could suppose that the second-order functions converge for the smallest separations, the observation of the fourth- and higher-order functions proves that this is certainly not the case. Figure 19 presents the two sets of functions of odd orders. They are clearly not equal at any separation, their ratios varying between 3 and 10, and over. Their shapes also differ greatly, the transverse functions presenting rather chaotic behaviour and the longitudinal functions a very regular one. They also differ markedly for the smallest separations: one may consider that the transverse functions should be falling to zero for $\Delta y/\eta < 3$ but the longitudinal functions have smooth shapes that clearly present no roll-off.

The autocorrelation coefficient functions of longitudinal and transverse separations are not equal at any scale (figure 20) but their normalizations make them converge towards 1 for the smallest separations. From their limit curvatures we can estimate the temperature 'Taylor microscales':

$$\lambda_{\theta\xi}^2 = -2 \Big/ \left[\frac{\partial^2}{\partial \Delta\xi^2} R_{\theta,\theta}(\Delta\xi) \right]_{\Delta\xi \to 0} \quad (\xi = x, y, t). \tag{31}$$

The plots of the derivatives with respect to separation of the time-and space-dependent functions (figure 21) show that we can get a good estimate of $\lambda_{\theta y} \approx 1{\cdot}90 \times 10^{-2}$ m; a less accurate estimate of $\lambda_{\theta x}$,

$$1{\cdot}08 \times 10^{-2} \text{ m} < \lambda_{\theta x} < 1{\cdot}36 \times 10^{-2} \text{ m}; \tag{32}$$

and only an upper limit on $\lambda_{\theta t}$ which indicates clearly that $\lambda_{\theta x}$ is smaller than $1{\cdot}7 \times 10^{-2}$ m. The value of $\lambda_{\theta x}$ obtained from the integral of the $\dot{\theta}$-spectrum by means of (6) is $1{\cdot}12 \times 10^{-2}$ m, in agreement with (32). So the estimated microscales $\lambda_{\theta x}$ and $\lambda_{\theta y}$ are clearly not equal, indicating that the isotropy assumption will not be verified, even at the smallest scales.

An interesting characteristic of the sheared inhomogeneous temperature fields is the non-zero derivative normalized third-moment or skewness factor S defined by (24). We present in figures 22–25 some data that illustrate the importance of this factor. To study its spectral behaviour we played back an analog record of temperature previously low-pass filtered at the Kolmogorov frequency N_{K}, differentiated the signal and squared the derivative in analog circuits before a new low-pass filtering at $2N_{\mathrm{K}}$ to take into account the contributions to frequencies higher than N_{K} possibly created by this pre-processing. The signals $\dot{\theta}$ and $\dot{\theta}^2$, sampled at a rate of $4N_{\mathrm{K}}$, were used to compute, with the complex Fourier transform routine, the *skewness cospectrum* (Wyngaard 1976) defined by

$$\int_0^\infty C_{\dot{\theta},\dot{\theta}^2}(k_1)\, dk_1 = \overline{\dot{\theta}^3}. \tag{33}$$

Actually, all the following results have been verified to be nearly identical when the computation is made with the temperature signal low-pass filtured at N_{K}, sampled at $2N_{\mathrm{K}}$ and digitally differentiated and squared.

Figure 22 presents the *skewness cospectrum* normalized by $\overline{\dot{\theta}^2}$. It appears to have a relatively high and constant value of the order of 1·3 over a large range of normalized wavenumbers, $10^{-3} < \eta k_1 < 4 \times 10^{-1}$, and to roll down to zero on both sides of this range. The *correlation-coefficient spectrum* of $\dot{\theta}$ and $\dot{\theta}^2$ (figure 23) has the same general shape, but stays non-negligible at lower wavenumbers. Yet in the large intermediate range it has small values, no more than 0·4, and about 0·2 in the range $10^{-2} < \eta k_1 < 6 \times 10^{-3}$. We must note that the rather abrupt roll-off of these two curves at $\eta k_1 = 1$

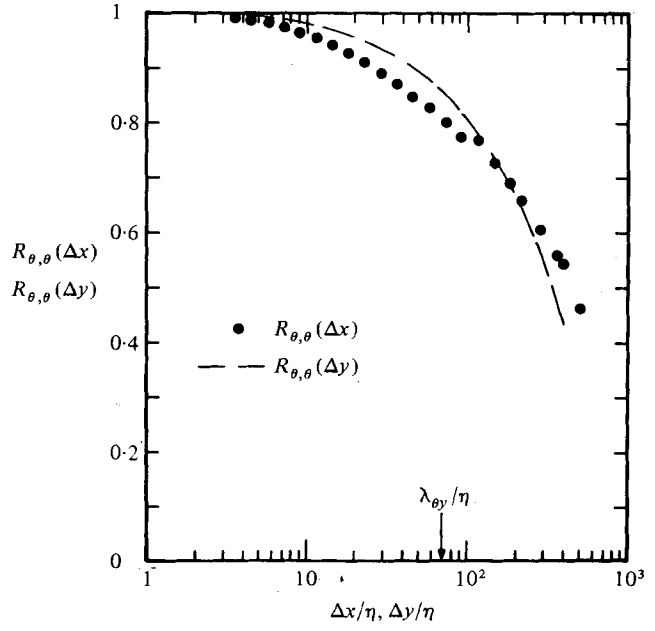

FIGURE 20. Longitudinal (●) and transverse (– –) temperature autocorrelation-coefficient functions.

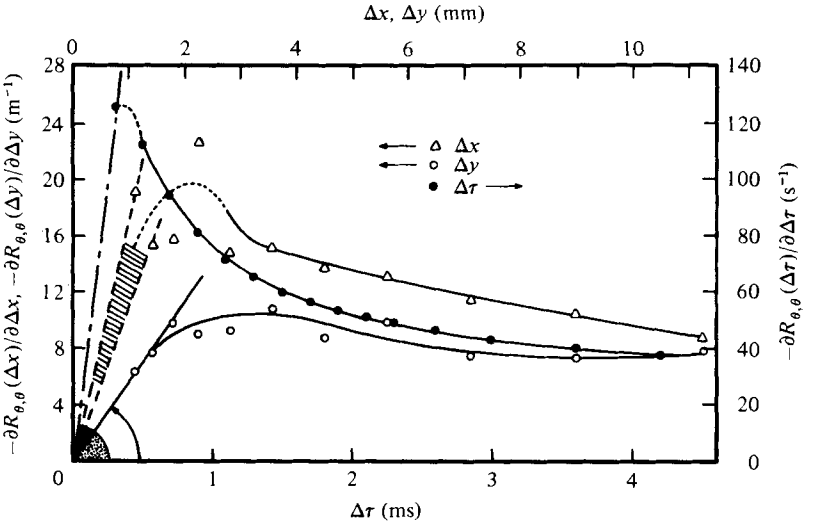

FIGURE 21. Derivatives of the longitudinal, transverse and time-dependent temperature autocorrelation functions.

is not necessarily a true feature of the field but can be due both to the probe resolution ($l \approx \eta$) and to the low-pass filtering at N_K; so we have no proof that these curves could not extend to even higher wavenumbers. Figure 24 displays the *skewness cospectrum* multiplied by ηk_1 and normalized by $\dot{\theta}$-variance, which indicates the contribution of each wavenumber to the skewness, as

$$(\ln 10) \int_0^\infty \frac{\eta k_1 C_{\dot{\theta},\dot{\theta}^2}(\eta k_1)\, d \log_{10} \eta k_1}{(\overline{\dot{\theta}^2})^{\frac{3}{2}}} = S(\dot{\theta}), \tag{34}$$

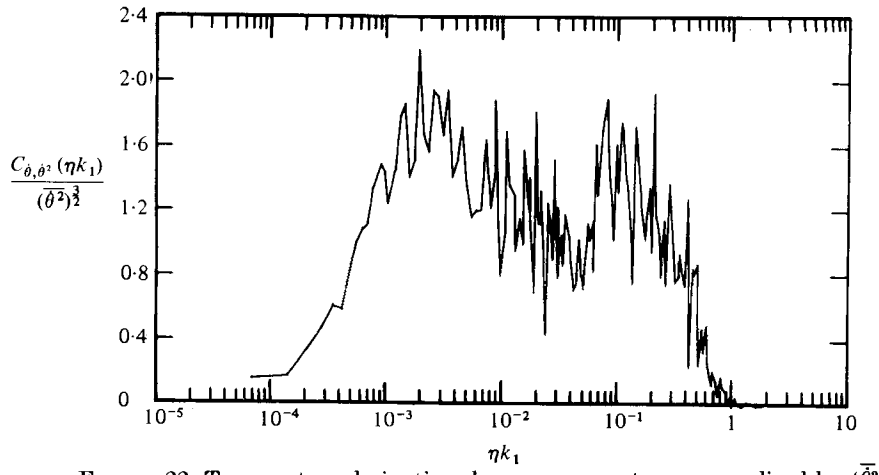

FIGURE 22. Temperature derivative skewness cospectrum normalized by $(\overline{\dot\theta^2})^{\frac{3}{2}}$.

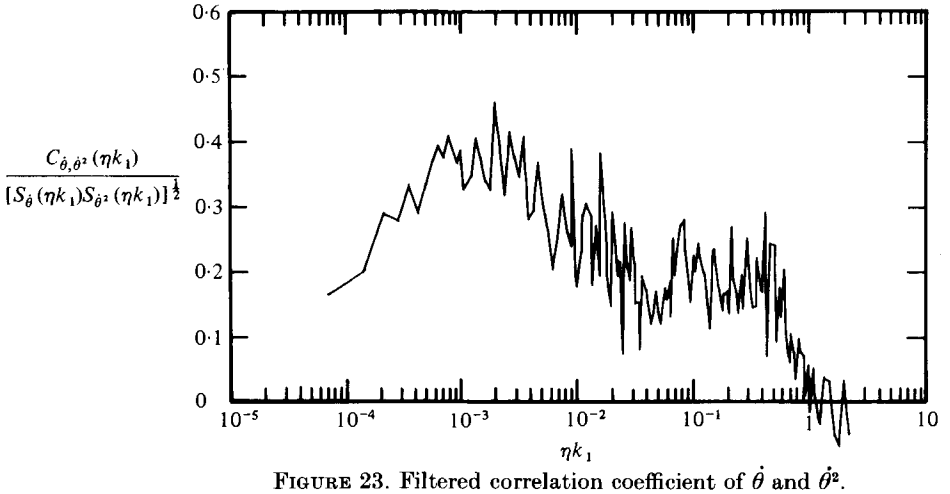

FIGURE 23. Filtered correlation coefficient of $\dot\theta$ and $\dot\theta^2$.

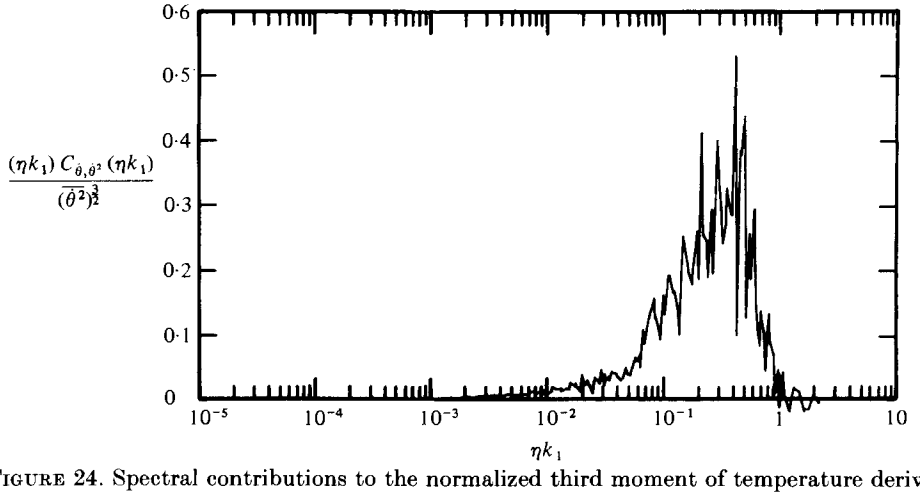

FIGURE 24. Spectral contributions to the normalized third moment of temperature derivative.

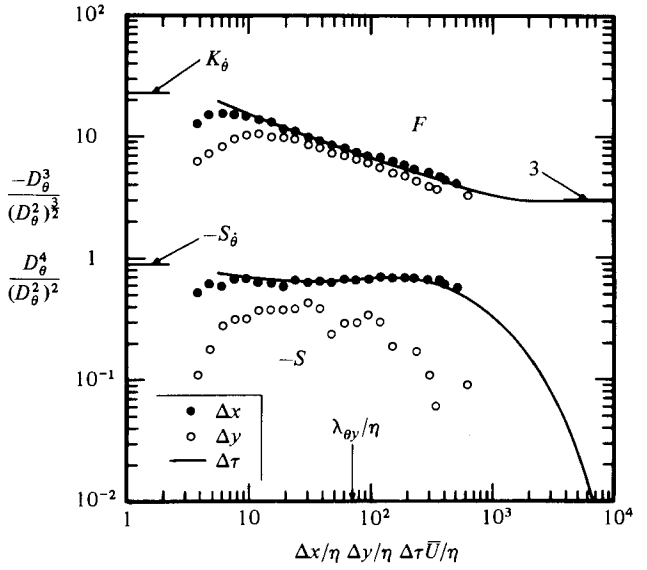

FIGURE 25. Skewness and flatness factors of temperature increments.

with $S(\dot\theta) \approx 0{\cdot}9$. This plot shows that 95% of the skewness of $\dot\theta$ is contributed by wavenumbers belonging to the range $5\times10^{-2} < \eta k_1 < 1$, i.e. those for which the dynamic field has been proved to verify the local isotropy assumption.

The velocity increment $\Delta u = u(\mathbf{x}+\Delta\xi) - u(\mathbf{x})$ is often considered as a velocity representative of structures of size $\Delta\boldsymbol{\xi}$ or as a velocity *spatially filtered* at the size and in the direction of $\Delta\boldsymbol{\xi}$. We can also consider the temperature increment $\Delta\theta$ as a *spatially filtered* temperature. The third-order structure functions normalized by the second-order structure functions thus appear to be the skewness factors of the temperatures $\Delta\theta$ *spatially filtered* in the direction $\Delta\xi$,

$$\frac{D_{\dot\theta}^3(\Delta\xi)}{[D_{\dot\theta}^2(\Delta\xi)]^{\frac{3}{2}}} = \frac{\overline{\Delta\theta^3(\Delta\xi)}}{[\overline{\Delta\theta^2(\Delta\xi)}]^{\frac{3}{2}}}, \tag{35}$$

and the normalized fourth-order structure functions appear to be their *flatness factors*. It is obvious that isotropy implies that the flatness factors of the temperature increments in the three directions be equal and that the skewness factors be zero. The evolutions of these skewness and flatness factors for longitudinal, transverse and time separations are presented in figure 25. Although there are noticeable differences between the longitudinal and time-dependent structure functions themselves (differences that will be shown and discussed elsewhere) it is worth noting the excellent agreement between the skewness and flatness factors for $\Delta x/h$ and $\Delta\tau\bar{U}/\eta$ (to be clear the space-dependent skewnesses are negative and the time-dependent ones positive). For large time lags the temperature increment behaves as a Gaussian variable ($S \to 0$, $F \approx 3$) and for the smallest time lags it seems to behave asymptotically as $\dot\theta$. The flatness factors for the longitudinal and transverse directions behave in almost parallel ways, but they are not equal and their differences seem to increase for the smaller separations. As for the skewnesses, they are not equal and they depart significantly from zero: the transverse skewness has a behaviour rather erratic (but less erratic than $D_{\dot\theta}^3(\Delta y)$) and could fall to negligible values for $\Delta y/\eta < 3$; in contrast the skewness of the longitudinal temperature increment keeps about the same value

of $-0{\cdot}7$ for all separations smaller than $\Delta x/\eta \approx 4 \times 10^2$, indicating a constancy of anisotropy.

8. Conclusions

This set of data obtained in a relatively high-Reynolds-number heated boundary layer with high-resolution probes and sophisticated data processing techniques allows us to draw several conclusions about the local isotropy assumption.

The spectra of u' and w', their correlation-coefficient spectrum, their spectral coherency, the transverse structure functions of u' and the time-dependent structure functions of w', the corresponding autocorrelations and the estimates of the transverse and longitudinal Taylor microscales, present consistent evidence that the assumption is satisfied in the dissipative range of scales smaller or equal to 20η ($\eta k_1 > 5 \times 10^{-2}$). The assumption does not seem to be satisfied in the 'inertial' subrange, where it was expected from the general criteria ($10^{-2} < \eta k_1 < 5 \times 10^{-2}$). Moreover, the spectra ϕ_3 and ϕ_1 do not follow exact $-\frac{5}{3}$ power laws in this range, but ϕ_1 is proportional to $k_1^{-\frac{5}{3}}$ in the subrange $2 \times 10^{-3} < \eta k_1 < 10^{-2}$ where the spectrum of turbulent kinetic-energy production is non-negligible and where isotropy is not satisfied. This result confirms the conclusions that we drew from a review of data obtained in high-Reynolds-number flows: isotropy is usually not observed in the 'inertial subrange' and does not seem to be closely connected with the approximately $-\frac{5}{3}$ power laws of spectra.

Direct comparisons of the longitudinal and transverse temperature autocorrelation and structure functions indicate that the local-isotropy assumption is not satisfied by temperature even for scales as small as 3η. This is also confirmed by the various estimates of the longitudinal and transverse Taylor temperature microscales. The spectral distribution of the derivative skewness ($S(\dot{\theta}) \approx 0{\cdot}9$) differs significantly from zero over a wide range of scales, $10^{-3} < \eta k_1 < 4 \times 10^{-1}$, and falls to zero only at wavenumbers close to $\eta k_1 = 1$ corresponding to the probe resolution and frequency filtering. 95% of the contributions to $S(\dot{\theta})$ are due to wavenumbers for which the velocity field agrees with the isotropy assumption. The evolution of the skewness and flatness factors of the temperature increments in the transverse and longitudinal directions confirm the non-agreement with the assumption. The constant value of the skewness of the increment in the longitudinal direction for all separations smaller than $\Delta x/\eta = 4 \times 10^2$ seems to indicate that the large-scale anisotropy of the field is conserved through the cascade down to very small scales.

The author wants to thank Prof. M. Coantic, scientific head of his program of researches, and all I.M.S.T. scientific and technical staff for their help and various contributions, P. Chambaud for his technical assistance in all measurements, B. Zucchini for the drawings and A. M. Rugiero for typing the manuscript; J. A. B. Wills and an unknown referee also contributed greatly to the improvement of this paper. This work was supported by the Centre National de la Recherche Scientifique, specifically under the A.T.P. Recherches Atmosphériques of I.N.A.G.

REFERENCES

Antonia, R. A., Chambers, A. J., Phong-Anant, D. & Rajagopalan, S. 1979 *Boundary-Layer Met.* **17**, 101.

Antonia, R. A. & Van Atta, C. W. 1978 *J. Fluid Mech.* **84**, 561.

ANTONIA, R. A. & VAN ATTA, C. W. 1979 *Phys. Fluids* **22**, 2430.

BATCHELOR, G. K. 1959 *J. Fluid Mech.* **5**, 113.

BRADSHAW, P. 1969 *Aero. Res. Counc. R. & M.* no. 36003, 5.

BUSCH, N. E. 1973 *Boundary-Layer Met.* **4**, 213.

CHAMPAGNE, F. H. 1978 *J. Fluid Mech.* **86**, 67.

CHAMPAGNE, F. H., FRIEHE, C. A., LA RUE, J. C. & WYNGAARD, J. C. 1977 *J. Atmos. Sci.* **34**, 515.

CHAMPAGNE, F. H., HARRIS, V. G. & CORRSIN, S. 1970 *J. Fluid Mech.* **41**, 81.

CHAMPAGNE, F. H., SLEICHER, C. A. & WEHRMANN, O. H. 1967 *J. Fluid Mech.* **86**, 67.

COANTIC, M., BONMARIN, P., POUCHAIN, B. & FAVRE, A. 1969 *AGARD Conf. Proc.* CP48, 17–0.

COANTIC, M., RAMAMONJIARISOA, A., MESTAYER, P., RESCH, F. & FAVRE, A. 1981 *J. Geophys. Res.* **86**, 6607.

CORRSIN, S. 1949 *J. Aero. Sci.* **16**, 757.

CORRSIN, S. 1952 *J. Appl. Phys.* **23**, 113.

CORRSIN, S. 1958 *NACA* RM 58B11.

DREYER, G. F. 1974 Ph.D. dissertation, University of California, San Diego.

DUNCKEL, M. L., HASSE, L., KRUGERMEYER, L., SCHRIEVER, D. & WUCKNITZ, J. 1974 *Boundary-Layer Met.* **6**, 81.

FREYMUTH, P. 1981 Kinematic and dimensional arguments on derivative skewness in turbulent shear flows. In *Proc. Joint A.S.M.E./A.S.C.E. Bioengineering, Fluids Engineering and Applied Mechanics Conf., June* 22–24, *Boulder.*

FREYMUTH, P. & UBEROI, M. S. 1971 *Phys. Fluids* **14**, 2574.

GARRATT, J. R. 1972 *Q. J. R. Met. Soc.* **98**, 642.

GIBSON, C. H., FRIEHE, C. A. & MCCONNELL, S. O. 1977 *Phys. Fluids Suppl.* **20**, S156.

GIBSON, C. H. & SCHWARZ, W. H. 1963 *J. Fluid Mech.* **16**, 365.

GIBSON, C. H., STEGEN, G. R. & WILLIAMS, R. B. 1970 *J. Fluid Mech.* **41**, 153.

GIBSON, M. M. 1962 *Nature* **195**, 1281.

GIBSON, M. M. 1963 *J. Fluid Mech.* **15**, 161.

HILL, R. J. 1978 *J. Fluid Mech.* **88**, 541.

LARCHEVÊQUE, M., CHOLLET, J. P., HERRING, J. R., LESIEUR, M., NEWMAN, G. R. & SCHERTZER, D. 1980 In *Turbulent Shear Flows* 2 (ed. L. J. S. Bradbury, F. Durst, B. E. Launder, F. W. Schmidt & J. H. Whitelaw). Springer.

KAIMAL, J. C., WYNGAARD, J. C., IZUMI, Y. & COTE, O. R. 1972 *Q. J. R. Met. Soc.* **98**, 563.

KLEBANOFF, P. S. 1953 *NACA Rep.* no. 1247.

KOLMOGOROV, A. N. 1941 *Dokl. Akad. Nauk S.S.S.R.* **30**, 301.

KOLMOGOROV, A. N. 1962 *J. Fluid Mech.* **13**, 1.

LARSEN, S. E. & BUSCH, N. E. 1974 *DISA Info.* **16**, 15.

LARSEN, S. E. & BUSCH, N. E. 1976 *DISA Info.* **20**, 5.

LAUFER, J. 1951 *NACA Rep.* no. 1033.

LEAVITT, E. 1975 *J. Phys. Oceanogr.* **5**, 157.

LUMLEY, J. L. 1965 *Phys. Fluids* **8**, 1056.

MCBEAN, G. A. & ELLIOTT, J. A. 1978 *J. Atmos. Sci.* **35**, 1890.

MESTAYER, P. 1975 Thèse de Docteur-Ingénieur, I.M.S.T., Université d'Aix-Marseille II, France.

MESTAYER, P. 1980 Thèse de Docteur ès Sciences Physiques, Université d'Aix-Marseille II, France.

MESTAYER, P. 1982 Spatial resolution of a multi- (non-identical) wire probe. (In preparation.)

MESTAYER, P. & CHAMBAUD, P. 1979 *Boundary-Layer Met.* **16**, 311.

MESTAYER, P. G., CHAMPAGNE, F. H., FRIEHE, C. A., LA RUE, J. C. & GIBSON, C. H. 1978 In *Turbulent Fluxes Through the Sea Surface, Wave Dynamics and Prediction* (ed. A. Favre & K. Hasselmann), p. 51. Plenum.

MESTAYER, P. G., GIBSON, C. H., COANTIC, M. F. & PATEL, A. S. 1976 *Phys. Fluids* **19**, 1279.

MESTAYER, P., PAGES, J. P., COANTIC, M. & SAISSAC, J. 1980 In *Proc. Joint Symp. on Heat and Mass Transfer and the Structure of Turbulence* (ed. Z. Zaric). Hemisphere.

MONIN, A. S. & YAGLOM, A. M. 1975 *Statistical Fluid Mechanics*, vol. 2. M.I.T. Press.

OBUKHOV, A. M. 1946 *Akad. Nauk S.S.S.R. Inst. Teor. Geofiz. Trudy* **1**, 95.

PAO, Y. H. 1965 *Phys. Fluids* **8**, 1063.

PARK, J. T. 1976 Ph.D. thesis, University of California, San Diego.

REVAULT D'ALLONNES, M. 1978 Thèse de Doctorat ès Sciences Physiques, Muséum National d'Histoire Naturelle de Paris, Université Pierre et Marie Curie (Paris VII), France.

SCHMITT, K. F., FRIEHE, C. A. & GIBSON, C. H. 1978*a* *Boundary-Layer Met.* **15**, 215.

SCHMITT, K. F., FRIEHE, C. A. & GIBSON, C. H. 1978*b* *J. Phys. Oceanogr.* **8**, 151.

SREENIVASAN, K. R., ANTONIA, R. A. & BRITZ, D. 1979 *J. Fluid Mech.* **94**, 745.

SREENIVASAN, K. R., ANTONIA, R. A. & DANH, H. Q. 1977 *Phys. Fluids* **20**, 1238.

SREENIVASAN, K. R. & TAVOULARIS, S. 1980 *J. Fluid Mech.* **101**, 783.

TANI, I. & KOBAYASHI, Y. 1952 In *Proc. 1st Japan Nat. Congr. Appl. Mech.* p. 465.

TAYLOR, G. I. 1935 In *Proc. R. Soc. Lond.* A**151**, 421.

TOWNSEND, A. A. 1948 *Austr. J. Sci. Res.* **1**, 161.

TOWNSEND, A. A. 1951 *Proc. Camb. Phil. Soc.* **47**, 375.

UBEROI, M. S. 1957 *J. Appl. Phys.* **28**, 1165.

UBEROI, M. S. & FREYMUTH, P. 1969 *Phys. Fluids* **12**, 1359.

UBEROI, M. S. & FREYMUTH, P. 1970 *Phys. Fluids* **13**, 2205.

VAN ATTA, C. W. 1977 *J. Fluid Mech.* **80**, 609.

WILLIAMS, R. M. & PAULSON, C. A. 1978 *J. Fluid Mech.* **83**, 547.

WYNGAARD, J. C. 1968 *J. Sci. Instrum.* **1**, 1105.

WYNGAARD, J. C. 1976 The maintenance of temperature derivative skewness in large Reynolds number flows. Unpublished manuscript.

WYNGAARD, J. C. & CLIFFORD, S. F. 1977 *J. Atmos. Sci.* **34**, 922.